# Tracing Earth's O2 evolution using Zn/Fe ratios in marine carbonates

# Tracing Earth's $O_2$ evolution using Zn/Fe ratios in marine carbonates

Xiao-Ming Liu[1,2*], Linda C. Kah[3], Andrew H. Knoll[4], Huan Cui[5],

Alan J. Kaufman[5], Anat Shahar[2], and Robert M. Hazen[2]

1. *Department of Geological Sciences, University of North Carolina, Chapel Hill, North Carolina, 27599 USA*
2. *Geophysical Laboratory, Carnegie Institution of Washington, Washington DC 20015, USA*
3. *Department of Earth and Planetary Sciences, University of Tennessee, Knoxville, Tennessee 37996, USA*
4. *Department of Organismic and Evolutionary Biology, Harvard University, Cambridge, Massachusetts 02138, USA*
5. *Department of Geology, University of Maryland, College Park, Maryland 20742, USA*

* Corresponding author:

Department of Geological Sciences
University of North Carolina
Chapel Hill, North Carolina, 27599 USA

Tel: (919) 926-0675
Email: xiaomliu@unc.edu

Word count for the text is 3100; 3 Figures

**Abstract**

Through Earth history, atmospheric oxygen has increased from initial values near zero to its present day level of about 21% by volume; concomitantly, changes in ocean redox conditions have fundamentally altered global biogeochemical cycles. While there is a reasonable understanding of where oxygen history begins and ends, the quantitative timetable of oxygenation that links the endpoints has proven contentious. Equilibrium between marine surface environments and the overlying atmosphere suggests that carbonate-based redox proxies could refine paleoredox records in time and space. Here we explore the use of Zn/Fe ratios to infer the evolution of atmospheric $O_2$ through time, based on marine carbonate rocks that are well characterized in terms of depositional age, environmental setting, and diagenetic history. While Fe and Zn in the shallow ocean is mainly sourced from hydrothermal inputs, their redox sensitivities differ significantly, so that geological intervals with higher $O_2$ would be characterized by stepped increases in Zn/Fe as preserved in shallow marine carbonates. Therefore, Zn/Fe analyses of ancient carbonates allow us to constrain past atmospheric $pO_2$ levels, providing a secular record of atmospheric $O_2$ over the past 3.5 billion years. In particular, we corroborate an earlier proposal that for much of the Proterozoic Eon, $O_2$ levels were as low as 0.1-1% of present atmospheric level. We conclude that Zn/Fe in shallow marine carbonate rocks has potential to provide a quantitative tracer for the long-term redox evolution of the oceans and the rise of atmospheric $O_2$.

## Introduction

Earth's $O_2$–rich atmosphere, unique among known planets, has played an essential role in evolving feedbacks between life and environment. Atmospheric $O_2$ was extremely low in the Archean Eon (>2.5 billion years ago), and while multiple lines of evidence suggest that Earth's oxygenation was protracted (Kah and Bartley, 2011; Kah et al., 2004; Lyons et al., 2014; Planavsky et al., 2014), $pO_2$ may have risen abruptly at two different points in time: first during the "Great Oxygenation Event" (GOE) at ~2.4 billion years (Ga) (Canfield, 2005; Farquhar et al., 2011; Guo et al., 2009; Holland, 2006), when atmospheric $O_2$ rose from <0.001% to an intermediate value commonly estimated as 1 to 10% of the current level (Farquhar et al., 2000; Pavlov and Kasting, 2002), and again during a "Neoproterozoic Oxygenation Event" (NOE) at ~800 to 542 million years ago (Canfield and Teske, 1996; Fike et al., 2006; Frei et al., 2009; Och and Shields-Zhou, 2012). The latter transition may well have continued into the Phanerozoic Eon, eventually resulting in near-present $O_2$ (Berner, 2006; Dahl et al., 2010; Sperling et al., 2015).

Redox-sensitive major and trace elements in iron formations and black shales deposited beneath euxinic waters have been developed as proxies to reconstruct paleoenvironmental history in deep time (Konhauser et al., 2009; Sahoo et al., 2012; Scott et al., 2008). The paucity of these facies in many Proterozoic successions, however, limits the continuity of current reconstructions of Earth's oxygenation. Here we provide evidence for the hypothesis that carbonate-based redox proxies can provide an independent estimate of past $pO_2$, expanding the paleo-redox record in time and space (Hardisty et al., 2014). Limestone and penecontemporaneous dolomites that retain depositional signatures well (Wilson et al., 2010) are abundant in the geologic record, typically recording shallow marine

environments that would have been in open communication with the overlying atmosphere. Paleoenvironmental research on carbonate rocks commonly focuses on individual stratigraphic successions; here we adopt a complementary strategy, analyzing a large suite of Phanerozoic, Proterozoic, and Archean samples that enables us to make statistical statements (Sperling et al., 2015) about Zn/Fe in the global surface ocean through geologic time. More importantly, we develop a new tool to provide quantitative constraints on atmospheric $pO_2$ through Earth history.

In the modern ocean, zinc input from hydrothermal ridge systems (~$4.4 \times 10^9$ mol/year) is an order of magnitude greater than riverine fluxes (~$3.4 \times 10^8$ mol/year) (Robbins et al., 2013). As an essential nutrient in many phytoplankton enzymes, especially those of eukaryotes (Williams and da Silva, 1996), zinc plays an important role in marine primary production, and for this reason, Zn is depleted in surface waters relative to the deep sea (Morel and Price, 2003). Zn concentrations in euxinic black shale and iron formations (Robbins et al., 2013; Scott et al., 2013), however, suggest that the bioavailability of Zn has not changed dramatically through Earth history. The Fe budget is similar to that of Zn, wherein hydrothermal input dominates over riverine fluxes by a factor of ~ 9 (Wheat et al., 2002)(Wheat et al., 2002)(Wheat et al., 2002)(Wheat et al., 2002)(Wheat et al., 2002)(Wheat et al., 2002). Under sulphidic conditions, dissolved $Zn^{2+}$ and $Fe^{2+}$ behave similarly and are rapidly precipitated as sulphides (Morse and Luther III, 1999). In addition, because both Fe and Zn behave as incompatible elements during mantle partial melting, Zn/Fe has been developed as a tracer of mantle redox, revealing that the oxygen fugacity of the upper mantle has remained relatively constant through Earth history (Lee et al., 2010). In the following discussion, we assume that Zn/Fe in hydrothermal inputs into the ocean have not changed

significantly through time. We recognize, however, that a number of factors could limit this assumption, and consider these below.

Zn/Fe in the sedimentary record thus has the potential to document Earth surface redox evolution if we consider the following assumptions: 1) Zn and Fe budgets in oceans are dominated by hydrothermal inputs and are therefore not significantly influenced by secular evolution of continental inputs; 2) $Fe^{2+}$ and $Zn^{2+}$ have similar solubility in oceans; 3) the partition coefficient of Zn/Fe ratios into carbonates have remained the same through time; and 4) when $Fe^{2+}$ is oxidized to $Fe^{3+}$, it precipitates from seawater and thus is not incorporated into carbonate; zinc, however, remains divalent as $Zn^{2+}$.

**Methods**

Major, trace, and REE concentrations were determined with a Thermo Scientific® iCAP-Q ICP-MS (Inductively Coupled Plasma – Mass Spectrometry) at the Carnegie Institution of Washington. Approximately 5 to 10 mg of micro-drilled sample powders were weighed and dissolved in 2 ml distilled 0.4 M $HNO_3$ and reacted for 12 hours. The resulting solutions were centrifuged for 5 minutes at ~6000 rps and 1 ml of the supernatant was pipetted and diluted with distilled 4 ml 0.4 M $HNO_3$ for elemental analysis. Calibration curves were created using multi-elemental standards with different dilution made from pure element solutions (Alfa Aesar®). Both standard and sample solutions were doped with 4 ppb In to correct for instrumental drift. Precision of the analyses was determined by repeated analyses of an in-house carbonate standard, and was typically better than 5% ($2\sigma$) for major elements, and better than 10% ($2\sigma$) for most trace elements including rare earth

elements (REEs). Accuracy of the analyses was determined by replicates of an international coral standard (JCp-1), as shown in Fig. S1.

## Results and discussion

Here, we report Zn/Fe molar ratios in marine carbonate rock through Earth history (Fig. 1) and provide a quantification of atmospheric $O_2$ evolution since the Mesoarchean Era. Samples (n = 1700) come from our analyses (n = 300), as well as a literature compilation (see Table S1). In all carbonate samples, the potential for diagenetic alteration is of concern. To evaluate the degree of sample alteration, we selected specimens with known sedimentological and stratigraphic context and investigated their petrography and elemental and isotope geochemistry. Samples used in this study were primarily composed of fine-grained limestone and penecontemporaenous, fabric-retentive dolostone, including both micrites and stromatolites. We micro-sampled carbonate specimens from polished billets to avoid weathering alteration, secondary veins/precipitation, and areas with visible non-carbonate phases. In addition to geological and petrographic criteria, we further selected samples based on primary isotopic and trace element patterns (see SI 2).

Even if we carefully select the most primary samples, we cannot ignore diagenetic influences on the elemental composition of sampled carbonates, as this can contribute to local variation of Zn/Fe (Fig. 1). Both Zn and Fe partition coefficient ($K_d$) from fluid to carbonates increase with increasing diagenesis as shown by earlier work of Brand and Veizer (1980). Also, $K_d$ (Fe) increases faster compared to $K_d$ (Zn), from 1 to 20 and from 5.2 to 5.5 for Fe and Zn, respectively. According to this work, diagenesis will cause decrease in Zn/Fe ratios by incorporating more Fe than Zn in carbonates. We acknowledge that all of the

carbonates examined here have undergone some degree of burial diagenesis, and this will be reflected in the variance of Zn/Fe within individual time intervals. Also, local primary production differences may contribute to Zn/Fe variability of different formations from the same interval. In the modern oxidized shallow ocean, particulate Fe sourced from eroding continents remains biogeochemically labile and may be cycled back to a dissolved phase during diagenesis in reducing continental margin sediments (Raiswell et al., 2006). Therefore, there is also a potentially large and variable source of reactive Fe to shallow marine settings that is decoupled from the Zn flux, which likely cause Zn/Fe ratios to be lower and therefore could contribute to the variations observed in Zn/Fe data. In addition, theoretical calculations suggest that kinetic effects on trace element partitioning in carbonate may contribute to Zn/Fe variability in samples from the same locality (DePaolo, 2011; Watson, 2004). Importantly, however, these influences should not result in systematic variations that would contribute to observed first-order secular changes. We plot all carbonate samples based on their lithology in Fig. S2; this shows that there is no systematic difference between limestone and dolomite samples through time -- not unexpected, as many Proterozoic dolomites formed penecontemporaneously and preserve geochemical signatures as well as coeval limestones that underwent neomorphism during burial.

We observe a distinct trend of increasing Zn/Fe through time (Fig. 1), especially around the GOE and NOE. Our Paleoproterozoic data are also consistent with earlier suggestions that $pO_2$ may have risen substantially during the GOE and then declined again to persistent Proterozoic values (Lyons et al., 2014). Employing three statistically complementary approaches (see details in SI 3), carbonate Zn/Fe could follow “step” or “smooth” fits through Earth’s history (Figs. S3, 4, & 5), where we prefer the “step” approach

with lognormal distributions (see Fig. 2 and SI 3). Using lognormal distributions to estimate Zn/Fe through time, we can provide quantitative constraints on Earth's atmospheric $O_2$ evolution, as follows.

From the chemical reaction of Fe oxidization from $Fe^{2+}$ to $Fe^{3+}$:

$$4Fe^{2+}\ (aq) + O_2\ (aq) + 10H_2O\ (aq) = 4Fe(OH)_3\ (s) + 8H^+\ (aq),$$

$$K = \frac{a^8_{(H^+)}}{a^{10}_{(H_2O)} \times a^4_{(Fe^{2+})} \times a_{(O_2)}} \quad [1],$$

where $K$ is the equilibrium constant and $\alpha$ is activity. In this equation, we assume that when $Fe^{2+}$ oxidizes to $Fe^{3+}$ and is precipitated from the aqueous system as iron hydroxide, only $Fe^{2+}$ gets incorporated into carbonates. We are aware that secular variations in seawater sulfate might modulate hydrothermal iron fluxes through time via the formation of iron sulfides (Kump and Seyfried, 2005), we do not know the extent to which Zn abundances might similarly be buffered and so do consider this in our first-order model. Assuming $O_2$ equilibrium between atmosphere and surface ocean on hundred million year time scales, we can write the equation using atmospheric oxygen fugacity, $f_{(O_2)}$, as

$$logK = 4log\frac{1}{a_{(Fe^{2+})}} - log\ f_{(O_2)} + log\frac{a^8_{(H^+)}}{a^{10}_{(H_2O)}} \quad [2],$$

if we assume the Zn concentrations in seawater and partitioning of Zn/Fe from seawater to carbonate minerals are constant over Earth history. Therefore, we can write the equation normalized to $Zn^{2+}$ as

$$logK = 4loga^P_{(Zn^{2+}/Fe^{2+})} - log\ f^P_{(O_2)} + log\frac{a^8_{(H^+)}}{a^{10}_{(H_2O)}}$$

$$logK = 4loga^{M}_{(Zn^{2+}/Fe^{2+})} - log\, f^{M}_{(O_2)} + log\frac{a^{8}_{(H^+)}}{a^{10}_{(H_2O)}} \quad [3],$$

in which superscripts P and M indicate the past and modern parameters. Assuming pH and K are constant (see SI 4), we can simplify the relationship between Fe/Zn ratios and $f_{(O_2)}$, as $f^{P}_{(O_2)} = r^4 \cdot f^{M}_{(O_2)}$ [4], where $f^{P}_{(O_2)}$ is the oxygen fugacity in the past (any time in Earth's history), $f^{M}_{(O_2)}$ is the oxygen fugacity in modern time, and

$$r = \frac{(Zn^{2+}/Fe^{2+})^{P}}{(Zn^{2+}/Fe^{2+})^{M}} \quad [5],$$

provides Zn/Fe ratios in past carbonate normalized to modern values. If we assume that atmospheric $O_2$ is in equilibrium with the shallow marine environment, and that we know the current atmospheric $P_{(O_2)}$ (0.21) and the modern seawater Zn/Fe ratios as reflected in Zn/Fe ratios of marine carbonates, we can use Zn/Fe to calculate $f_{(O_2)}$ at any given time of Earth history (Fig. 3). This $f_{(O_2)}$ curve provides a more continuous coverage of atmospheric $O_2$ levels compared to compilations derived from multiple geochemical tracers, such as mass-independent S isotopes and paleosol records (Catling and Claire, 2005; Rye and Holland, 1998).

The $logf_{(O_2)}$ curve in Fig. 3 reproduces what we think we know about oxygen history: estimated $pO_2$ is extremely low in the Archean and reaches modern levels only in the mid-Paleozoic Era. Moreover, the estimates match our current understanding (Lyons et al., 2014) of a general two-step increase of atmospheric $O_2$ around the GOE and the NOE. Importantly, our study provides an estimate of the upper and lower bounds on $pO_2$ in the mid-Proterozoic atmosphere, with a preferred value between 0.1 and 1% PAL. This value is substantially lower than traditional estimates based on paleosol work (Canfield, 1998; Rye and Holland,

1998), but consistent with recent estimates based on an independent tracer, a kinetic model for Cr-Mn oxidation and Cr isotopes in ironstones (Planavsky et al., 2014). We conducted sensitivity tests of temperature and pH variations on our $pO_2$ estimates and found that the influence of temperature is negligible. pH, however, could potentially lower $pO_2$ estimates, especially for earlier samples when $pCO_2$ was high (see SI 4 for details); thus, our estimates of Proterozoic $pO_2$ should be considered conservative and may overestimate past oxygen levels. There are hints of biologically interesting structure in the Neoproterozoic and Cambrian records, but at present our sample numbers and bin sizes are too small to address this in detail. As more carbonate data become available for key transitional time periods such as those around GOE and NOE, potentially complex secular patterns of redox change may become clearer. Further investigations on well-constrained modern and Phanerozoic marine carbonates are currently underway to evaluate with more quantitative rigor the potential effects of diagenesis, mineralogy, and ocean depth gradients distributions on the proxy proposed here.

## Conclusion

In summary, we have demonstrated the potential for using divalent cations in carbonates as sensitive proxies for the evolution of Earth's near surface environment. Because many marine carbonate rocks were deposited in shallow marine environments, in direct contact with the atmosphere, elemental ratios are likely to reflect equilibrium atmospheric conditions extending back to the Archean Eon and including time intervals poorly represented by other lithologies. Although further work will be needed to fully validate this promising paleo-redox proxy, carbonate-based redox proxies show great

potential to expand the paleoredox record and to provide self-consistent and quantitative constraints on atmospheric $O_2$ through Earth's history.

Figure Captions

**Figure 1.** Zn/Fe molar ratios versus time for individual carbonate analyses. The figure contains ~1700 measurements of Zn/Fe data, including literature data (blue), and our 300 new analyses (orange).

**Figure 2.** Zn/Fe molar ratio versus time for carbonates, averaged by formation. Formation averages (orange diamonds) were calculated based on simple arithmetic mean of samples within the same formation. Median (orange) and mean from lognormal distribution (blue) lines were calculated based on all samples from the designated time intervals. Estimated Zn/Fe ratio curve through Earth's history. Uncertainties (light blue fields) are estimated based on one standard deviation from the lognormal distribution.

**Figure 3.** Estimated atmospheric $f_{(O_2)}$ through Earth's history. The orange line indicates the best estimate (mean values from lognormal distribution) from carbonate Zn/Fe ratios from this study (yellow fields show the upper and lower range of estimated $O_2$, which is calculated based on one sigma of lognormal distributions). The blue field indicates semi-quantitative interpretation from current understanding of the atmospheric $O_2$ curve (modified from Lyons et al. (2014)).

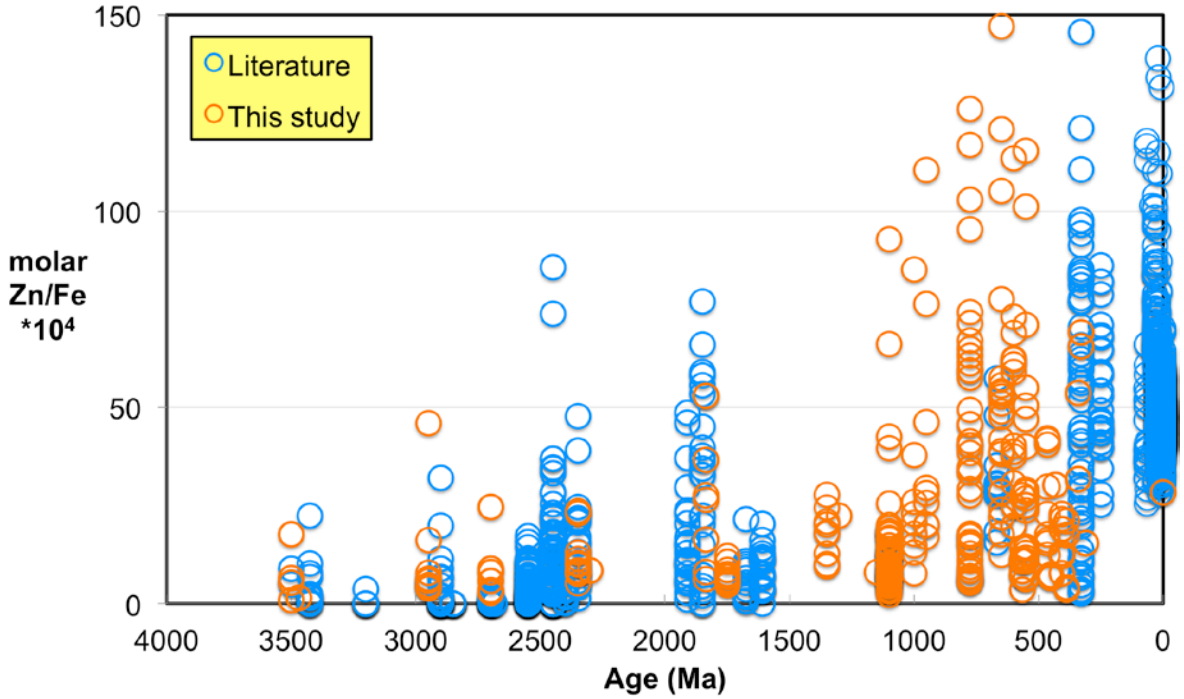
Literature
This study
molar Zn/Fe *10⁴
150
100
50
0
4000
3500
3000
2500
2000
1500
1000
500
0
Age (Ma)

Figure 1.

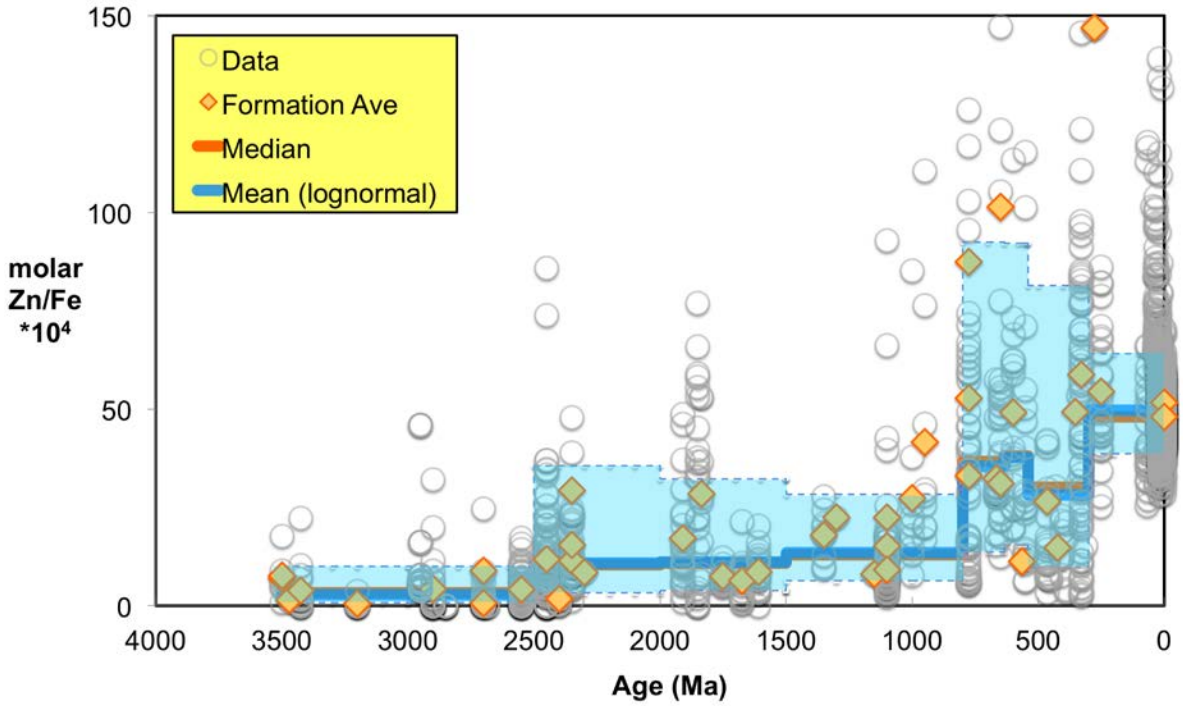


221

222 Figure 2.

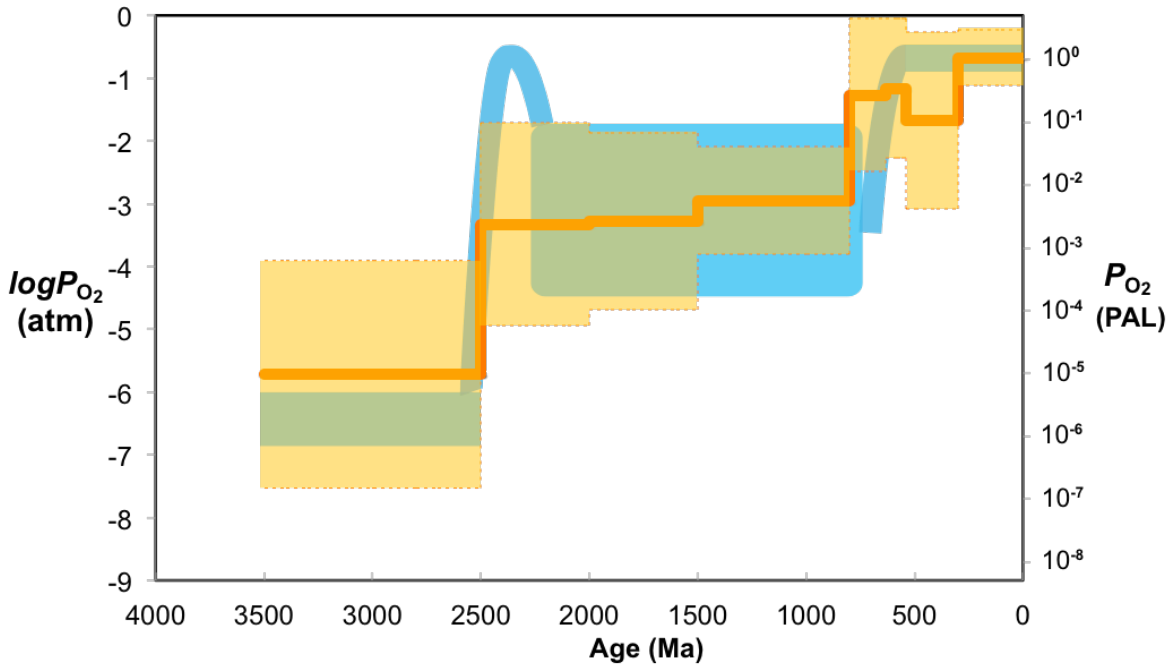


223

224 Figure 3.

## References


Berner, R.A., 2006. GEOCARBSULF: A combined model for Phanerozoic atmospheric $O_2$ and $CO_2$. Geochimica et Cosmochimica Acta, 70(23): 5653-5664.

Brand, U., Veizer, J., 1980. Chemical diagenesis of a multicomponent carbonate system; 1, Trace elements. Journal of Sedimentary Research, 50(4): 1219-1236.

Canfield, D.E., 1998. A new model for Proterozoic ocean chemistry. Nature, 396(6710): 450-453.

Canfield, D.E., 2005. The early history of atmospheric oxygen: Homage to Robert A. Garrels. Annual Review of Earth and Planetary Sciences, 33: 1-36.

Canfield, D.E., Teske, A., 1996. Late Proterozoic rise in atmospheric oxygen concentration inferred from phylogenetic and sulphur-isotope studies. Nature, 382(6587): 127-132.

Catling, D.C., Claire, M.W., 2005. How Earth's atmosphere evolved to an oxic state: A status report. Earth and Planetary Science Letters, 237(1–2): 1-20.

Dahl, T.W. et al., 2010. Devonian rise in atmospheric oxygen correlated to the radiations of terrestrial plants and large predatory fish. Proceedings of the National Academy of Sciences of the United States of America, 107(42): 17911-17915.

DePaolo, D.J., 2011. Surface kinetic model for isotopic and trace element fractionation during precipitation of calcite from aqueous solutions. Geochimica et Cosmochimica Acta, 75(4): 1039-1056.

Farquhar, J., Bao, H.M., Thiemens, M., 2000. Atmospheric influence of Earth's earliest sulfur cycle. Science, 289(5480): 756-758.

Farquhar, J., Zerkle, A., Bekker, A., 2011. Geological constraints on the origin of oxygenic photosynthesis. Photosynthesis Research, 107(1): 11-36.

Fike, D.A., Grotzinger, J.P., Pratt, L.M., Summons, R.E., 2006. Oxidation of the Ediacaran Ocean. Nature, 444(7120): 744-747.

Frei, R., Gaucher, C., Poulton, S.W., Canfield, D.E., 2009. Fluctuations in Precambrian atmospheric oxygenation recorded by chromium isotopes. Nature, 461(7261): 250-U125.

Guo, Q.J. et al., 2009. Reconstructing Earth's surface oxidation across the Archean-Proterozoic transition. Geology, 37(5): 399-402.

Hardisty, D.S. et al., 2014. An iodine record of Paleoproterozoic surface ocean oxygenation. Geology.

Holland, H.D., 2006. The oxygenation of the atmosphere and oceans. Philosophical Transactions of the Royal Society B: Biological Sciences, 361(1470): 903-915.

Kah, L.C., Bartley, J.K., 2011. Protracted oxygenation of the Proterozoic biosphere. International Geology Review, 53(11-12): 1424-1442.

Kah, L.C., Lyons, T.W., Frank, T.D., 2004. Low marine sulphate and protracted oxygenation of the proterozoic biosphere. Nature, 431(7010): 834-838.

Konhauser, K.O. et al., 2009. Oceanic nickel depletion and a methanogen famine before the Great Oxidation Event. Nature, 458(7239): 750-753.

Lee, C.T.A. et al., 2010. The redox state of arc mantle using Zn/Fe systematics. Nature, 468(7324): 681-685.

Lyons, T.W., Reinhard, C.T., Planavsky, N.J., 2014. The rise of oxygen in Earth's early ocean and atmosphere. Nature, 506(7488): 307-315.

Morel, F.M.M., Price, N.M., 2003. The Biogeochemical Cycles of Trace Metals in the Oceans. Science, 300(5621): 944-947.
Morse, J.W., Luther III, G.W., 1999. Chemical influences on trace metal-sulfide interactions in anoxic sediments. Geochimica et Cosmochimica Acta, 63(19–20): 3373-3378.
Och, L.M., Shields-Zhou, G.A., 2012. The Neoproterozoic oxygenation event: Environmental perturbations and biogeochemical cycling. Earth-Science Reviews, 110(1–4): 26-57.
Pavlov, A.A., Kasting, J.F., 2002. Mass-independent fractionation of sulfur isotopes in Archean sediments: Strong evidence for an anoxic Archean atmosphere. Astrobiology, 2(1): 27-41.
Planavsky, N.J. et al., 2014. Low Mid-Proterozoic atmospheric oxygen levels and the delayed rise of animals. Science, 346(6209): 635-638.
Raiswell, R. et al., 2006. Contributions from glacially derived sediment to the global iron (oxyhydr)oxide cycle: Implications for iron delivery to the oceans. Geochimica et Cosmochimica Acta, 70(11): 2765-2780.
Robbins, L.J. et al., 2013. Authigenic iron oxide proxies for marine zinc over geological time and implications for eukaryotic metallome evolution. Geobiology, 11(4): 295-306.
Rye, R., Holland, H.D., 1998. Paleosols and the evolution of atmospheric oxygen: A critical review. American Journal of Science, 298(8): 621-672.
Sahoo, S.K. et al., 2012. Ocean oxygenation in the wake of the Marinoan glaciation. Nature, 489(7417): 546-549.
Scott, C. et al., 2008. Tracing the stepwise oxygenation of the Proterozoic ocean. Nature, 452(7186): 456-U5.
Scott, C. et al., 2013. Bioavailability of zinc in marine systems through time. Nature Geoscience, 6(2): 125-128.
Sperling, E.A. et al., 2015. The global record of iron geochemical data from Proterozoic through Paleozoic basins. Nature in revision.
Watson, E.B., 2004. A conceptual model for near-surface kinetic controls on the trace-element and stable isotope composition of abiogenic calcite crystals. Geochimica et Cosmochimica Acta, 68(7): 1473-1488.
Wheat, C.G., Mottl, M.J., Rudnicki, M., 2002. Trace element and REE composition of a low-temperature ridge-flank hydrothermal spring. Geochimica et Cosmochimica Acta, 66(21): 3693-3705.
Williams, R.J.P., da Silva, J.J.R.F., 1996. The natural selection of the chemical elements. Great Britian, Bath Press Ltd.
Wilson, J.P. et al., 2010. Geobiology of the late Paleoproterozoic Duck Creek Formation, Western Australia. Precambrian Research, 179(1-4): 135-149.

**Acknowledgements**

We are grateful to T. Mock for assistance with the Q-ICP-MS analyses, and M. Horan for help in the clean lab. We thank Mahrnaz Siahy and Axel Hofmann for providing the Pongola samples. We are grateful to M. Van Kranendonk for sampling help in Western Australia and M. Evans, J. Hao, T. Lyons, D. Sverjensky and J. Veizer for discussions. We thank anonymous reviewers and executive editor Eric Oelkers for their constructive comments. The Alfred P. Sloan Foundation, the Deep Carbon Observatory, the National Science Foundation, the NASA Astrobiology Institute, and the Carnegie Institution of Washington provided financial support to RMH and X-ML. AHK thanks the NASA Astrobiology Institute.

**Author Contributions**

X-ML and RMH designed the project with inputs from all authors. X-ML performed the chemical analyses. X-ML wrote the manuscript with inputs from all authors. LK, AHK, HC, AJK, and RMH provided samples.

**Competing financial interests**

The authors declare no competing financial interests.

**Figure Captions**

**Figure 1.** Zn/Fe molar ratios versus time for individual carbonate analyses. The figure contains ~1700 measurements of Zn/Fe data, including literature data (blue), and our 320 new analyses (orange).

**Figure 2.** Zn/Fe molar ratio versus time for carbonates averaged by formation. Formation averages (orange diamonds) were calculated based on simple arithmetic mean of samples within the same formation. Median (orange) and mean from lognormal distribution (blue) lines were calculated based on all samples from the designated time periods. Estimated Zn/Fe ratio curve through Earth's history. Uncertainties (yellow fields) are estimated based on one standard deviation from the lognormal distribution.

**Figure 3.** Estimated atmospheric $f_{(O_2)}$ through Earth's history. The orange line indicates the best estimate (mean values from lognormal distribution) from carbonate Zn/Fe ratios from this study (yellow fields show the upper and lower range of estimated $O_2$, which is calculated based on one sigma of lognormal distributions). The blue field indicates semi-quantitative interpretation from current understanding of the atmospheric $O_2$ curve (modified from Lyons et al. (2014)).

154

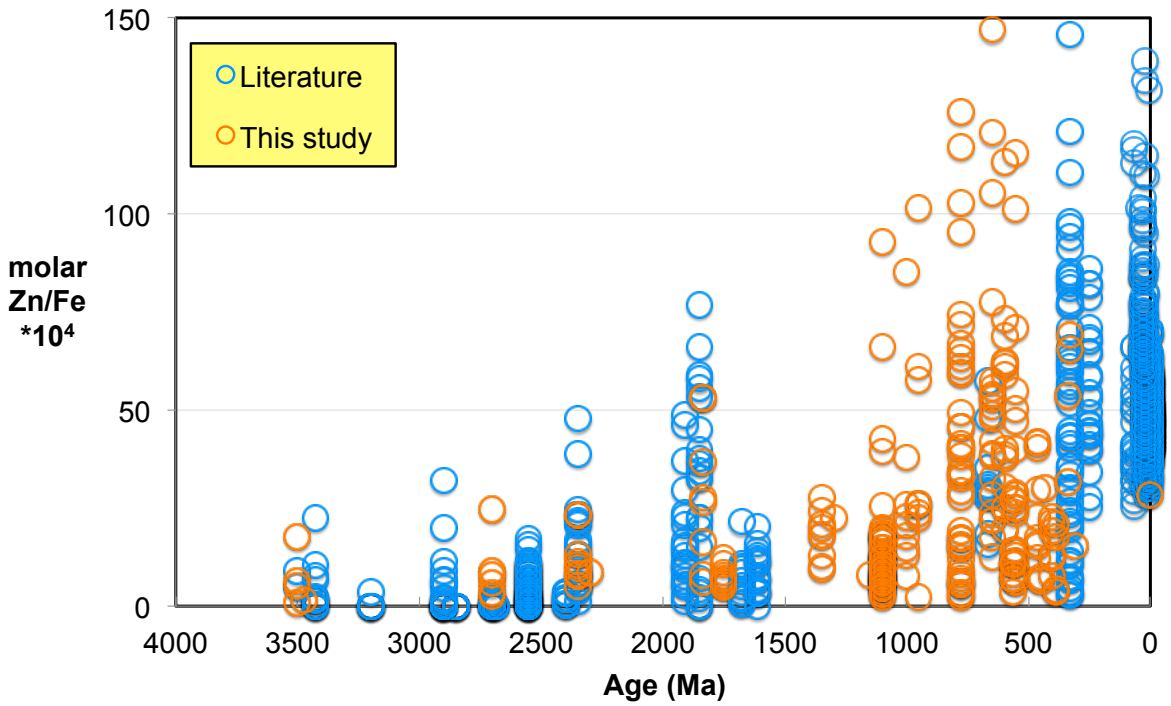


155

156 Figure 1.

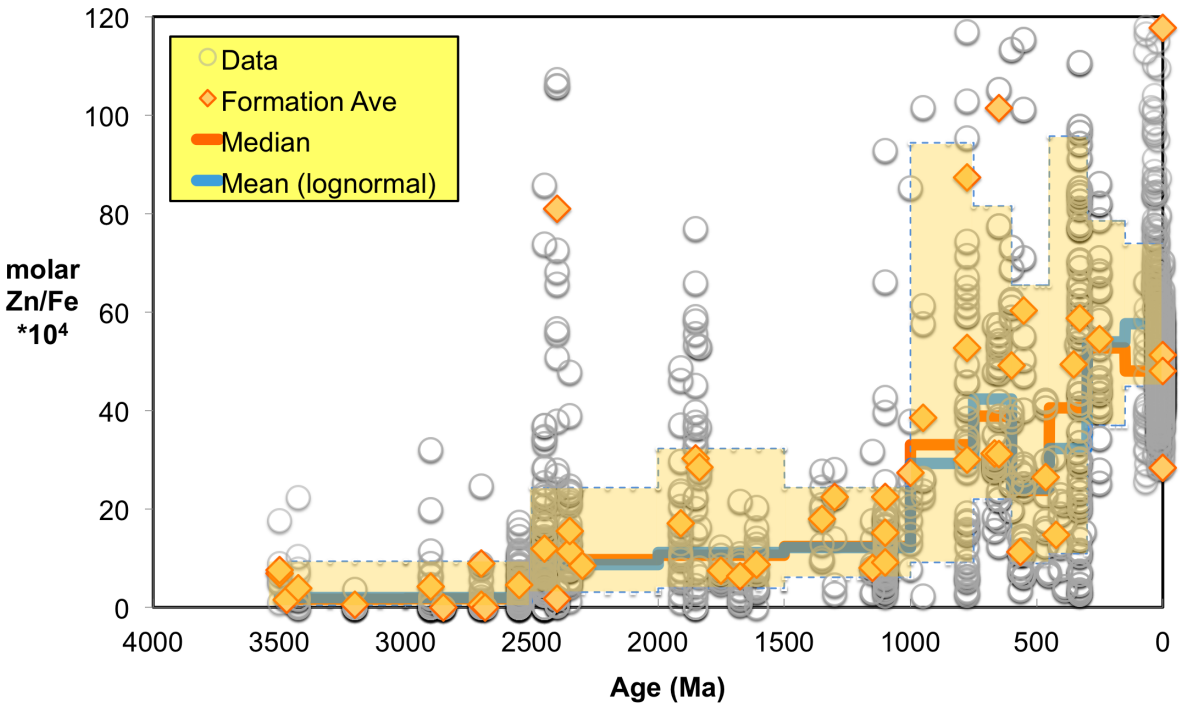


157

158

159 Figure 2.

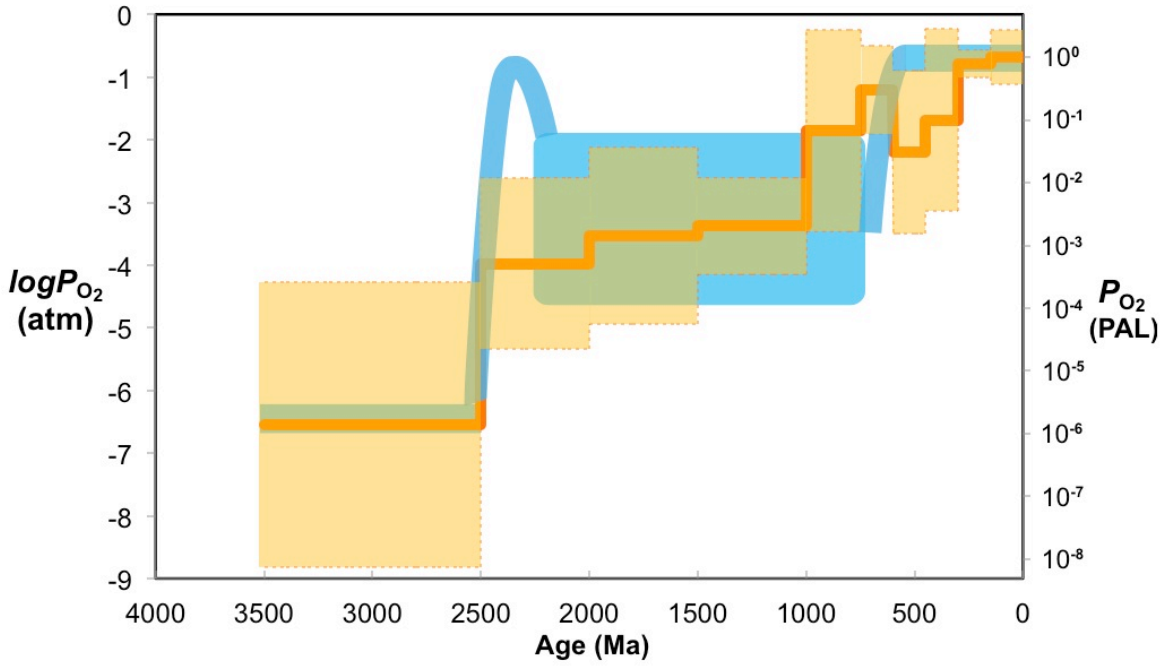


160

161 Figure 3.

## Supplementary Information

### *SI 1. Tables*

***Table S1. Zn/Fe ratios with sample name and age information from this study.***

| Geologic Unit | Sample # | Age (Ma) | Zn/Fe $*10^4$ | Reference |
|---|---|---|---|---|
| Strelley Pool Fm, Warrawoona Group, Pilbara, Western Australia | BH2 | 3400 | 0.9 | Hazen collection |
| Strelley Pool Fm, Warrawoona Group, Pilbara, Western Australia | BH3 | 3400 | 17.6 | Hazen collection |
| Strelley Pool Fm, Warrawoona Group, Pilbara, Western Australia | BH7 | 3400 | 5.3 | Hazen collection |
| Calcite filling in Mt. Ada basalt | BH18 | 3470 | 1.5 | Hazen collection |
| Pongola Fm, South Africa | Po1 | 2950 | 16.1 | Beukes and Lowe 1989 |
| Pongola Fm, South Africa | Po2 | 2950 | 45.9 | Beukes and Lowe 1989 |
| Pongola Fm, South Africa | Po3 | 2950 | 4.5 | Beukes and Lowe 1989 |
| Pongola Fm, South Africa | Po4 | 2950 | 6.4 | Beukes and Lowe 1989 |
| Pongola Fm, South Africa | Po5 | 2950 | 5.9 | Beukes and Lowe 1989 |
| Pongola Fm, South Africa | Po6 | 2950 | 7.8 | Beukes and Lowe 1989 |
| Pongola Fm, South Africa | Po7 | 2950 | 5.8 | Beukes and Lowe 1989 |
| Pongola Fm, South Africa | Po8 | 2950 | 4.0 | Beukes and Lowe 1989 |
| Pongola Fm, South Africa | Po9 | 2950 | 3.8 | Beukes and Lowe 1989 |
| Pongola Fm, South Africa | Po10 | 2950 | 4.8 | Beukes and Lowe 1989 |
| Tumbiana Fm, Fortesue Group, Western Australia | BH10 | 2700 | 6.5 | Hazen collection |
| Tumbiana Fm, Fortesue Group, Western Australia | BH12 | 2700 | 24.6 | Hazen collection |
| Tumbiana Fm, Fortesue Group, Western Australia | BH13 | 2700 | 8.9 | Hazen collection |
| Tumbiana Fm, Fortesue Group, Western Australia | BH14 | 2700 | 8.0 | Hazen collection |
| Tumbiana Fm, Fortesue Group, Western Australia | BH15 | 2700 | 2.8 | Hazen collection |
| Tumbiana Fm, Fortesue Group, Western Australia | BH16 | 2700 | 3.4 | Hazen collection |
| Kazput Fm, Turee Creek, Australia | AN94 | 2350 | 7.6 | Knoll et al. unpublished |
| Kazput Fm, Turee Creek, Australia | AN95 | 2350 | 8.4 | Knoll et al. unpublished |
| Kazput Fm, Turee Creek, Australia | AN96 | 2350 | 9.9 | Knoll et al. unpublished |
| Kazput Fm, Turee Creek, Australia | AN97 | 2350 | 7.7 | Knoll et al. unpublished |
| Kazput Fm, Turee Creek, Australia | AN98 | 2350 | 8.2 | Knoll et al. unpublished |
| Kazput Fm, Turee Creek, Australia | AN99 | 2350 | 5.2 | Knoll et al. unpublished |
| Kazput Fm, Turee Creek, Australia | AN100 | 2350 | 7.8 | Knoll et al. unpublished |
| Kazput Fm, Turee Creek, Australia | AN101 | 2350 | 10.4 | Knoll et al. unpublished |
| Kazput Fm, Turee Creek, Australia | AN102 | 2350 | 11.5 | Knoll et al. unpublished |
| Kazput Fm, Turee Creek, Australia | AN103 | 2350 | 13.1 | Knoll et al. unpublished |
| Kazput Fm, Turee Creek, Australia | AN104 | 2350 | 23.0 | Knoll et al. unpublished |
| Kazput Fm, Turee Creek, Australia | AN105 | 2350 | 23.5 | Knoll et al. unpublished |
| Kazput Fm, Turee Creek, Australia | BH19 | 2350 | 8.5 | Hazen collection |
| Duck Creek, Australia | AN80 | 1835 | 53.0 | Wilson et al. 2010 |
| Duck Creek, Australia | AN82 | 1835 | 8.0 | Wilson et al. 2010 |
| Duck Creek, Australia | AN83 | 1835 | 36.6 | Wilson et al. 2010 |

| | | | | |
|---|---|---|---|---|
| Duck Creek, Australia | AN84 | 1835 | 53.0 | Wilson et al. 2010 |
| Duck Creek, Australia | AN85 | 1835 | 26.5 | Wilson et al. 2010 |
| Duck Creek, Australia | AN86 | 1835 | 16.2 | Wilson et al. 2010 |
| Duck Creek, Australia | AN87 | 1835 | 27.6 | Wilson et al. 2010 |
| Duck Creek, Australia | AN88 | 1835 | 6.2 | Wilson et al. 2010 |
| Vempalle Fm, Cuddapah Basin, India | V-SC/1 | 1750 | 8.5 | Chakrabarti et al. 2013 |
| Vempalle Fm, Cuddapah Basin, India | V-SC/2 | 1750 | 4.8 | Chakrabarti et al. 2013 |
| Vempalle Fm, Cuddapah Basin, India | V-SC/3 | 1750 | 5.3 | Chakrabarti et al. 2013 |
| Vempalle Fm, Cuddapah Basin, India | V-SC/5 | 1750 | 10.6 | Chakrabarti et al. 2013 |
| Vempalle Fm, Cuddapah Basin, India | V-SC/6-1 | 1750 | 6.8 | Chakrabarti et al. 2013 |
| Vempalle Fm, Cuddapah Basin, India | V-P2/1 | 1750 | 5.5 | Chakrabarti et al. 2013 |
| Vempalle Fm, Cuddapah Basin, India | V-P8/1 | 1750 | 12.2 | Chakrabarti et al. 2013 |
| Vempalle Fm, Cuddapah Basin, India | V-P10/1 | 1750 | 7.5 | Chakrabarti et al. 2013 |
| Vempalle Fm, Cuddapah Basin, India | V-P11/1 | 1750 | 6.9 | Chakrabarti et al. 2013 |
| Vempalle Fm, Cuddapah Basin, India | V-P12/1 | 1750 | 6.1 | Chakrabarti et al. 2013 |
| Kyrpy Group, East European Platform, Southern Urals, Russia | C133-3252.3 | 1350 | 17.8 | Kah et al. 2007 |
| Kyrpy Group, East European Platform, Southern Urals, Russia | C133-3253.3 | 1350 | 12.8 | Kah et al. 2007 |
| Kyrpy Group, East European Platform, Southern Urals, Russia | C133-3038 | 1350 | 9.5 | Kah et al. 2007 |
| Kyrpy Group, East European Platform, Southern Urals, Russia | C133-2767.5 | 1350 | 27.7 | Kah et al. 2007 |
| Kyrpy Group, East European Platform, Southern Urals, Russia | C133-3114.5 | 1350 | 20.1 | Kah et al. 2007 |
| Kyrpy Group, East European Platform, Southern Urals, Russia | C203-3852A | 1350 | 24.4 | Kah et al. 2007 |
| Kyrpy Group, East European Platform, Southern Urals, Russia | C203-2459.8 | 1350 | 10.0 | Kah et al. 2007 |
| Kyrpy Group, East European Platform, Southern Urals, Russia | C203-2459.6-1 | 1350 | 18.1 | Kah et al. 2007 |
| Kyrpy Group, East European Platform, Southern Urals, Russia | C203-2353 | 1350 | 20.9 | Kah et al. 2007 |
| Sulky Fm, Dismal Lakes, Canada | DL1-364-1 | 1300 | 13.9 | Kah et al. 2006 |
| Sulky Fm, Dismal Lakes, Canada | DL1-306-1 | 1300 | 28.0 | Kah et al. 2006 |
| Sulky Fm, Dismal Lakes, Canada | DL1-332 | 1300 | 22.4 | Kah et al. 2006 |
| Sulky Fm, Dismal Lakes, Canada | SL16-1-1 | 1300 | 2.7 | Kah et al. 2006 |
| Sulky Fm, Dismal Lakes, Canada | SL17-10-1 | 1300 | 4.5 | Kah et al. 2006 |
| Avzyan Fm, Southern Urals, Russia | M1(AZ)-39 | 1150 | 3.0 | Bartley et al. 2007 |
| Avzyan Fm, Southern Urals, Russia | M1(AZ)-47 | 1150 | 31.7 | Bartley et al. 2007 |
| Avzyan Fm, Southern Urals, Russia | RV(AZ)-15 | 1150 | 8.8 | Bartley et al. 2007 |
| Avzyan Fm, Southern Urals, Russia | RV(AZ)-33 | 1150 | 13.8 | Bartley et al. 2007 |
| Avzyan Fm, Southern Urals, Russia | KT(AZ)-49.5 | 1150 | 17.6 | Bartley et al. 2007 |
| Avzyan Fm, Southern Urals, Russia | KT(AZ)-131.6 | 1150 | 3.0 | Bartley et al. 2007 |
| Avzyan Fm, Southern Urals, Russia | KT(AZ)-236-1 | 1150 | 7.0 | Bartley et al. 2007 |
| Avzyan Fm, Southern Urals, Russia | KT(AZ)-373.5 | 1150 | 8.0 | Bartley et al. 2007 |
| El Mreiti,Atar Group, West Africa | F4-10-1 | 1100 | 42.6 | Gilleaudeau and Kah 2013 |
| El Mreiti,Atar Group, West Africa | F4-19-1 | 1100 | 17.7 | Gilleaudeau and Kah 2013 |
| El Mreiti,Atar Group, West Africa | F4-50-1 | 1100 | 13.9 | Gilleaudeau and Kah 2013 |
| El Mreiti,Atar Group, West Africa | F4-53-1 | 1100 | 16.4 | Gilleaudeau and Kah 2013 |
| El Mreiti,Atar Group, West Africa | F4-90-1 | 1100 | 17.8 | Gilleaudeau and Kah 2013 |
| El Mreiti,Atar Group, West Africa | F4-95-1 | 1100 | 11.9 | Gilleaudeau and Kah 2013 |
| El Mreiti,Atar Group, West Africa | F4-98-1 | 1100 | 17.7 | Gilleaudeau and Kah 2013 |
| El Mreiti,Atar Group, West Africa | F4-99-1 | 1100 | 39.6 | Gilleaudeau and Kah 2013 |

| | | | | |
|---|---|---|---|---|
| El Mreiti,Atar Group, West Africa | F4-102-1 | 1100 | 20.0 | Gilleaudeau and Kah 2013 |
| El Mreiti,Atar Group, West Africa | F4-104-1 | 1100 | 8.6 | Gilleaudeau and Kah 2013 |
| El Mreiti,Atar Group, West Africa | F4-106-1 | 1100 | 11.4 | Gilleaudeau and Kah 2013 |
| El Mreiti,Atar Group, West Africa | F4-107-1 | 1100 | 13.0 | Gilleaudeau and Kah 2013 |
| El Mreiti,Atar Group, West Africa | F4-108-1 | 1100 | 6.8 | Gilleaudeau and Kah 2013 |
| El Mreiti,Atar Group, West Africa | F4-109-1 | 1100 | 6.1 | Gilleaudeau and Kah 2013 |
| El Mreiti,Atar Group, West Africa | F4-113-1 | 1100 | 13.1 | Gilleaudeau and Kah 2013 |
| El Mreiti,Atar Group, West Africa | F4-114-1 | 1100 | 7.2 | Gilleaudeau and Kah 2013 |
| El Mreiti,Atar Group, West Africa | F4-115-1 | 1100 | 7.8 | Gilleaudeau and Kah 2013 |
| El Mreiti,Atar Group, West Africa | F4-116-1 | 1100 | 7.8 | Gilleaudeau and Kah 2013 |
| El Mreiti,Atar Group, West Africa | F4-117-1 | 1100 | 7.9 | Gilleaudeau and Kah 2013 |
| Atar Group, West Africa | ATS-31 | 1100 | 14.8 | Kah et al. 2012 |
| Atar Group, West Africa | ATS-53 | 1100 | 92.9 | Kah et al. 2012 |
| Atar Group, West Africa | ATS-61 | 1100 | 16.5 | Kah et al. 2012 |
| Atar Group, West Africa | ATS-5-1 | 1100 | 13.8 | Kah et al. 2012 |
| Atar Group, West Africa | ATS-119 | 1100 | 11.6 | Kah et al. 2012 |
| Atar Group, West Africa | ATS-154 | 1100 | 12.8 | Kah et al. 2012 |
| Atar Group, West Africa | ATD-17 | 1100 | 18.4 | Kah et al. 2012 |
| Atar Group, West Africa | ATD-61 | 1100 | 18.2 | Kah et al. 2012 |
| Atar Group, West Africa | ATL-51-1 | 1100 | 9.3 | Kah et al. 2012 |
| Atar Group, West Africa | ATL-58 | 1100 | 66.2 | Kah et al. 2012 |
| Atar Group, West Africa | ATL-68 | 1100 | 4.9 | Kah et al. 2012 |
| Atar Group, West Africa | ATL-105 | 1100 | 19.3 | Kah et al. 2012 |
| Atar Group, West Africa | ATL-110-1 | 1100 | 6.3 | Kah et al. 2012 |
| Atar Group, West Africa | ATD-27.5 | 1100 | 12.3 | Kah et al. 2012 |
| Atar Group, West Africa | ATD-45 | 1100 | 18.4 | Kah et al. 2012 |
| Atar Group, West Africa | R1-Δ-1 | 1100 | 16.4 | Manning-Berg and Kah in prep |
| Atar Group, West Africa | R1-Δ-7 | 1100 | 25.5 | Manning-Berg and Kah in prep |
| Atar Group, West Africa | R1-Δ-13 | 1100 | 14.9 | Manning-Berg and Kah in prep |
| Atar Group, West Africa | R1-Δ-25 | 1100 | 12.7 | Manning-Berg and Kah in prep |
| Atar Group, West Africa | R1-Δ-29 | 1100 | 12.0 | Manning-Berg and Kah in prep |
| Atar Group, West Africa | R1-Δ-30 | 1100 | 10.3 | Manning-Berg and Kah in prep |
| Atar Group, West Africa | R1-Δ-31 | 1100 | 5.8 | Manning-Berg and Kah in prep |
| Atar Group, West Africa | R1-Δ-38 | 1100 | 12.2 | Manning-Berg and Kah in prep |
| Atar Group, West Africa | R1-Δ-39 | 1100 | 6.5 | Manning-Berg and Kah in prep |
| Atar Group, West Africa | R1-Δ-41 | 1100 | 9.6 | Manning-Berg and Kah in prep |
| Atar Group, West Africa | R1-Δ-42 | 1100 | 6.7 | Manning-Berg and Kah in prep |
| Atar Group, West Africa | R1-Δ-48 | 1100 | 8.1 | Manning-Berg and Kah in prep |
| Atar Group, West Africa | R1-Δ-54-1 | 1100 | 9.6 | Manning-Berg and Kah in prep |
| Atar Group, West Africa | R1-Δ-55 | 1100 | 7.1 | Manning-Berg and Kah in prep |
| Atar Group, West Africa | R1-Δ-58 | 1100 | 7.6 | Manning-Berg and Kah in prep |
| Atar Group, West Africa | R1-Δ-60 | 1100 | 4.7 | Manning-Berg and Kah in prep |
| Atar Group, West Africa | R1-Δ-61 | 1100 | 4.6 | Manning-Berg and Kah in prep |
| Atar Group, West Africa | R1-Δ-65 | 1100 | 9.9 | Manning-Berg and Kah in prep |
| Atar Group, West Africa | R1-Δ-68-1 | 1100 | 18.3 | Manning-Berg and Kah in prep |
| Atar Group, West Africa | R1-Δ-72 | 1100 | 6.6 | Manning-Berg and Kah in prep |
| Atar Group, West Africa | R1-Δ-76 | 1100 | 12.4 | Manning-Berg and Kah in prep |
| Atar Group, West Africa | R1-Δ-79-1 | 1100 | 8.3 | Manning-Berg and Kah in prep |
| Atar Group, West Africa | R1-Δ-81-1 | 1100 | 5.2 | Manning-Berg and Kah in prep |
| Atar Group, West Africa | R1-Δ-85 | 1100 | 6.0 | Manning-Berg and Kah in prep |
| Atar Group, West Africa | R1-Δ-89 | 1100 | 16.8 | Manning-Berg and Kah in prep |
| Atar Group, West Africa | R1-Δ-90 | 1100 | 4.4 | Manning-Berg and Kah in prep |
| Atar Group, West Africa | R1-Δ-97 | 1100 | 3.1 | Manning-Berg and Kah in prep |
| Atar Group, West Africa | R1-Δ-98 | 1100 | 9.2 | Manning-Berg and Kah in prep |

| | | | | |
|---|---|---|---|---|
| Atar Group, West Africa | R1-Δ-100 | 1100 | 3.6 | Manning-Berg and Kah in prep |
| Atar Group, West Africa | R1-Δ-103 | 1100 | 3.1 | Manning-Berg and Kah in prep |
| Atar Group, West Africa | R1-Δ-106 | 1100 | 2.2 | Manning-Berg and Kah in prep |
| Chattisgarh Supergroup, India | SRJ-2I | 1000 | 25.9 | Bickford et al. 2011 |
| Chattisgarh Supergroup, India | SRJ-3I | 1000 | 22.8 | Bickford et al. 2011 |
| Chattisgarh Supergroup, India | SRJ-4I | 1000 | 13.0 | Bickford et al. 2011 |
| Chattisgarh Supergroup, India | SRJ-6I | 1000 | 20.6 | Bickford et al. 2011 |
| Chattisgarh Supergroup, India | SRJ-8I | 1000 | 37.8 | Bickford et al. 2011 |
| Chattisgarh Supergroup, India | SRJ-9I | 1000 | 85.2 | Bickford et al. 2011 |
| Chattisgarh Supergroup, India | TML-3I | 1000 | 7.7 | Bickford et al. 2011 |
| Chattisgarh Supergroup, India | TML-6I | 1000 | 17.8 | Bickford et al. 2011 |
| Chattisgarh Supergroup, India | TML-7I | 1000 | 14.9 | Bickford et al. 2011 |
| Sukhaya Tunguska Formation, Russia | AN59 | 950 | 29.5 | Sergeev et al. 1997 |
| Sukhaya Tunguska Formation, Russia | AN60 | 950 | 46.1 | Sergeev et al. 1997 |
| Sukhaya Tunguska Formation, Russia | AN61 | 950 | 25.7 | Sergeev et al. 1997 |
| Sukhaya Tunguska Formation, Russia | AN62 | 950 | 76.4 | Sergeev et al. 1997 |
| Sukhaya Tunguska Formation, Russia | AN63 | 950 | 110.5 | Sergeev et al. 1997 |
| Sukhaya Tunguska Formation, Russia | AN64 | 950 | 17.0 | Sergeev et al. 1997 |
| Sukhaya Tunguska Formation, Russia | AN66 | 950 | 28.1 | Sergeev et al. 1997 |
| Sukhaya Tunguska Formation, Russia | AN67 | 950 | 20.0 | Sergeev et al. 1997 |
| Sukhaya Tunguska Formation, Russia | AN68 | 950 | 20.2 | Sergeev et al. 1997 |
| Akademikerbeen Group, Spitsbergen | AN1 | 775 | 29.2 | Knoll and Swett 1990 |
| Akademikerbeen Group, Spitsbergen | AN2 | 775 | 40.3 | Knoll and Swett 1990 |
| Akademikerbeen Group, Spitsbergen | AN3 | 775 | 17.3 | Knoll and Swett 1990 |
| Akademikerbeen Group, Spitsbergen | AN4 | 775 | 6.2 | Knoll and Swett 1990 |
| Akademikerbeen Group, Spitsbergen | AN5 | 775 | 63.2 | Knoll and Swett 1990 |
| Akademikerbeen Group, Spitsbergen | AN6 | 775 | 65.0 | Knoll and Swett 1990 |
| Akademikerbeen Group, Spitsbergen | AN7 | 775 | 27.6 | Knoll and Swett 1990 |
| Akademikerbeen Group, Spitsbergen | AN8 | 775 | 74.3 | Knoll and Swett 1990 |
| Akademikerbeen Group, Spitsbergen | AN9 | 775 | 95.4 | Knoll and Swett 1990 |
| Akademikerbeen Group, Spitsbergen | AN10 | 775 | 59.4 | Knoll and Swett 1990 |
| Akademikerbeen Group, Spitsbergen | AN12 | 775 | 71.5 | Knoll and Swett 1990 |
| Akademikerbeen Group, Spitsbergen | AN13 | 775 | 15.8 | Knoll and Swett 1990 |
| Akademikerbeen Group, Spitsbergen | AN14 | 775 | 49.4 | Knoll and Swett 1990 |
| Akademikerbeen Group, Spitsbergen | AN16 | 775 | 15.1 | Knoll and Swett 1990 |
| Akademikerbeen Group, Spitsbergen | AN18 | 775 | 17.6 | Knoll and Swett 1990 |
| Akademikerbeen Group, Spitsbergen | AN19 | 775 | 9.4 | Knoll and Swett 1990 |
| Akademikerbeen Group, Spitsbergen | AN20 | 775 | 34.4 | Knoll and Swett 1990 |
| Akademikerbeen Group, Spitsbergen | AN21 | 775 | 276.2 | Knoll and Swett 1990 |
| Akademikerbeen Group, Spitsbergen | AN22 | 775 | 34.6 | Knoll and Swett 1990 |
| Limestone-Dolomite Series, East Greenland | AN24 | 775 | 126.1 | Knoll et al. 1986 |
| Limestone-Dolomite Series, East Greenland | AN25 | 775 | 59.3 | Knoll et al. 1986 |
| Limestone-Dolomite Series, East Greenland | AN26 | 775 | 45.7 | Knoll et al. 1986 |
| Limestone-Dolomite Series, East Greenland | AN28 | 775 | 5.3 | Knoll et al. 1986 |
| Limestone-Dolomite Series, East Greenland | AN29 | 775 | 61.2 | Knoll et al. 1986 |
| Limestone-Dolomite Series, East Greenland | AN30 | 775 | 307.6 | Knoll et al. 1986 |
| Limestone-Dolomite Series, East Greenland | AN31 | 775 | 310.7 | Knoll et al. 1986 |
| Limestone-Dolomite Series, East Greenland | AN32 | 775 | 38.3 | Knoll et al. 1986 |
| Limestone-Dolomite Series, East Greenland | AN33 | 775 | 33.3 | Knoll et al. 1986 |
| Limestone-Dolomite Series, East Greenland | AN34 | 775 | 15.5 | Knoll et al. 1986 |
| Limestone-Dolomite Series, East Greenland | AN35 | 775 | 8.3 | Knoll et al. 1986 |
| Limestone-Dolomite Series, East Greenland | AN36 | 775 | 102.9 | Knoll et al. 1986 |
| Limestone-Dolomite Series, East Greenland | AN37 | 775 | 67.0 | Knoll et al. 1986 |
| Limestone-Dolomite Series, East Greenland | AN38 | 775 | 41.4 | Knoll et al. 1986 |

| | | | | |
|---|---|---|---|---|
| Shaler Group, Arctic Canada | AN41 | 775 | 5.6 | Jones et al. 2010 |
| Shaler Group, Arctic Canada | AN42 | 775 | 17.3 | Jones et al. 2010 |
| Shaler Group, Arctic Canada | AN43 | 775 | 45.7 | Jones et al. 2010 |
| Shaler Group, Arctic Canada | AN44 | 775 | 7.0 | Jones et al. 2010 |
| Shaler Group, Arctic Canada | AN45 | 775 | 154.8 | Jones et al. 2010 |
| Shaler Group, Arctic Canada | AN46 | 775 | 6.2 | Jones et al. 2010 |
| Shaler Group, Arctic Canada | AN47 | 775 | 40.3 | Jones et al. 2010 |
| Shaler Group, Arctic Canada | AN48 | 775 | 14.8 | Jones et al. 2010 |
| Shaler Group, Arctic Canada | AN49 | 775 | 116.9 | Jones et al. 2010 |
| Shaler Group, Arctic Canada | AN50 | 775 | 8.4 | Jones et al. 2010 |
| Shaler Group, Arctic Canada | AN51 | 775 | 10.9 | Jones et al. 2010 |
| Shaler Group, Arctic Canada | AN52 | 775 | 57.5 | Jones et al. 2010 |
| Shaler Group, Arctic Canada | AN53 | 775 | 6.9 | Jones et al. 2010 |
| Shaler Group, Arctic Canada | AN54 | 775 | 6.0 | Jones et al. 2010 |
| Shaler Group, Arctic Canada | AN55 | 775 | 12.8 | Jones et al. 2010 |
| Shaler Group, Arctic Canada | AN56 | 775 | 17.8 | Jones et al. 2010 |
| Lagoa Do Jacare Formation, Brazil | KM7-14.0.0 | 650 | 38.1 | Misi, A. et al., 2007 |
| Lagoa Do Jacare Formation, Brazil | KM7-14-01.0 | 650 | 21.9 | Misi, A. et al., 2007 |
| Lagoa Do Jacare Formation, Brazil | KM7-14-02.0 | 650 | 49.0 | Misi, A. et al., 2007 |
| Lagoa Do Jacare Formation, Brazil | KM7-14-03.0 | 650 | 17.6 | Misi, A. et al., 2007 |
| Lagoa Do Jacare Formation, Brazil | KM7-14-04.0 | 650 | 12.5 | Misi, A. et al., 2007 |
| Lagoa Do Jacare Formation, Brazil | KM7-14-05.0 | 650 | 22.0 | Misi, A. et al., 2007 |
| Lagoa Do Jacare Formation, Brazil | KM7-14-06.0 | 650 | 38.9 | Misi, A. et al., 2007 |
| Lagoa Do Jacare Formation, Brazil | KM7-14-07.0 | 650 | 54.1 | Misi, A. et al., 2007 |
| Lagoa Do Jacare Formation, Brazil | KM7-14-08.0 | 650 | 32.8 | Misi, A. et al., 2007 |
| Lagoa Do Jacare Formation, Brazil | KM7-14-09.0 | 650 | 23.8 | Misi, A. et al., 2007 |
| Huttenburg Fm, Namibia | S86A-971.2 | 650 | 105.2 | Kaufman et al., 2009 |
| Huttenburg Fm, Namibia | S86A-976.0 | 650 | 77.5 | Kaufman et al., 2009 |
| Huttenburg Fm, Namibia | S86A-977.0 | 650 | 120.9 | Kaufman et al., 2009 |
| Huttenburg Fm, Namibia | S86A-980.8 | 650 | 53.5 | Kaufman et al., 2009 |
| Huttenburg Fm, Namibia | S86A-985.1 | 650 | 147.1 | Kaufman et al., 2009 |
| Huttenburg Fm, Namibia | S86A-987.8 | 650 | 28.4 | Kaufman et al., 2009 |
| Huttenburg Fm, Namibia | S86A-988.2 | 650 | 41.8 | Kaufman et al., 2009 |
| Huttenburg Fm, Namibia | S86A-1033.8 | 650 | 424.1 | Kaufman et al., 2009 |
| Huttenburg Fm, Namibia | S86A-1060.2 | 650 | 156.2 | Kaufman et al., 2009 |
| Huttenburg Fm, Namibia | S86A-1077.1 | 650 | 57.4 | Kaufman et al., 2009 |
| Huttenburg Fm, Namibia | S86A-1144.8 | 650 | 52.8 | Kaufman et al., 2009 |
| Huttenburg Fm, Namibia | S86A-1145.1 | 650 | 47.7 | Kaufman et al., 2009 |
| Huttenburg Fm, Namibia | S86A-1148.4 | 650 | 55.6 | Kaufman et al., 2009 |
| Huttenburg Fm, Namibia | S86A-1213.2 | 650 | 51.1 | Kaufman et al., 2009 |
| Dhaiqa Fm, NW Arabian shield, Saudi Arabia | Dhaiqa-7 | 600 | 61.0 | Miller et al. 2008 |
| Dhaiqa Fm, NW Arabian shield, Saudi Arabia | Dhaiqa-21 | 600 | 62.5 | Miller et al. 2008 |
| Dhaiqa Fm, NW Arabian shield, Saudi Arabia | Dhaiqa-26 | 600 | 30.7 | Miller et al. 2008 |
| Dhaiqa Fm, NW Arabian shield, Saudi Arabia | Dhaiqa-34 | 600 | 37.5 | Miller et al. 2008 |
| Dhaiqa Fm, NW Arabian shield, Saudi Arabia | Dhaiqa-38 | 600 | 19.8 | Miller et al. 2008 |
| Dhaiqa Fm, NW Arabian shield, Saudi Arabia | Dhaiqa-38b | 600 | 40.1 | Miller et al. 2008 |
| Dhaiqa Fm, NW Arabian shield, Saudi Arabia | Dhaiqa-39 | 600 | 38.7 | Miller et al. 2008 |
| Dhaiqa Fm, NW Arabian shield, Saudi Arabia | Dhaiqa-46 | 600 | 24.9 | Miller et al. 2008 |
| Dhaiqa Fm, NW Arabian shield, Saudi Arabia | Dhaiqa-49 | 600 | 59.0 | Miller et al. 2008 |
| Dhaiqa Fm, NW Arabian shield, Saudi Arabia | Dhaiqa-51 | 600 | 19.8 | Miller et al. 2008 |
| Dhaiqa Fm, NW Arabian shield, Saudi Arabia | Dhaiqa-54 | 600 | 24.9 | Miller et al. 2008 |
| Dhaiqa Fm, NW Arabian shield, Saudi Arabia | M1-with fossil | 600 | 62.2 | Miller et al. 2008 |
| Dhaiqa Fm, NW Arabian shield, Saudi Arabia | N-2-3 | 600 | 113.4 | Miller et al. 2008 |
| Dhaiqa Fm, NW Arabian shield, Saudi Arabia | N-2-11 | 600 | 73.1 | Miller et al. 2008 |

| | | | | |
|---|---|---|---|---|
| Dhaiqa Fm, NW Arabian shield, Saudi Arabia | N-2-16 | 600 | 68.9 | Miller et al. 2008 |
| Yangjiaping, Doushantuo Fm, South China | YD-01 | 551 | 12.9 | Cui et al. 2015 |
| Yangjiaping, Doushantuo Fm, South China | YD-02 | 551 | 47.1 | Cui et al. 2015 |
| Yangjiaping, Doushantuo Fm, South China | YD-03 | 551 | 11.7 | Cui et al. 2015 |
| Yangjiaping, Doushantuo Fm, South China | YD-04 | 551 | 25.1 | Cui et al. 2015 |
| Yangjiaping, Doushantuo Fm, South China | YD-05 | 551 | 71.0 | Cui et al. 2015 |
| Yangjiaping, Doushantuo Fm, South China | YD-06 | 551 | 13.9 | Cui et al. 2015 |
| Yangjiaping, Doushantuo Fm, South China | YD-07 | 551 | 28.4 | Cui et al. 2015 |
| Yangjiaping, Doushantuo Fm, South China | YD-08 | 551 | 6.6 | Cui et al. 2015 |
| Yangjiaping, Doushantuo Fm, South China | YD-09 | 551 | 6.2 | Cui et al. 2015 |
| Yangjiaping, Doushantuo Fm, South China | YD-10 | 551 | 26.9 | Cui et al. 2015 |
| Yangjiaping, Doushantuo Fm, South China | YD-11 | 551 | 50.4 | Cui et al. 2015 |
| Yangjiaping, Doushantuo Fm, South China | YD-12 | 551 | 25.1 | Cui et al. 2015 |
| Yangjiaping, Doushantuo Fm, South China | YD-13 | 551 | 23.7 | Cui et al. 2015 |
| Yangjiaping, Doushantuo Fm, South China | YD-14 | 551 | 55.0 | Cui et al. 2015 |
| Yangjiaping, Doushantuo Fm, South China | YD-15 | 551 | 115.4 | Cui et al. 2015 |
| Yangjiaping, Doushantuo Fm, South China | YD-16 | 551 | 221.5 | Cui et al. 2015 |
| Yangjiaping, Doushantuo Fm, South China | YD-17 | 551 | 253.8 | Cui et al. 2015 |
| Yangjiaping, Doushantuo Fm, South China | YD-18 | 551 | 195.9 | Cui et al. 2015 |
| Yangjiaping, Doushantuo Fm, South China | YD-19 | 551 | 101.2 | Cui et al. 2015 |
| Yangjiaping, Doushantuo Fm, South China | YD-20 | 551 | 14.5 | Cui et al. 2015 |
| Yangjiaping, Doushantuo Fm, South China | YD-21 | 551 | 10.9 | Cui et al. 2015 |
| Yangjiaping, Doushantuo Fm, South China | YD-22 | 551 | 29.1 | Cui et al. 2015 |
| Yangjiaping, Doushantuo Fm, South China | YD-23 | 551 | 40.1 | Cui et al. 2015 |
| Orthoceras limestone, Ohio | BH21 | 465 | 27.5 | Hazen collection |
| Bryozoan limestone, Ohio | BH24 | 465 | 7.2 | Hazen collection |
| Branch Hill limestone, Ohio | BH25 | 465 | 10.9 | Hazen collection |
| Jersey Shore Station, Pennsylvania | BH26 | 465 | 7.0 | Hazen collection |
| Madison County, Kentucky | BH31 | 465 | 14.3 | Hazen collection |
| Ripley, Ohio | BH36 | 465 | 8.3 | Hazen collection |
| Washington, Kentucky | BH37 | 465 | 11.4 | Hazen collection |
| Bryozoan limestone, Ohio | BH33 | 465 | 3.5 | Hazen collection |
| Coburn Fm, Pennsylvania | BH41 | 465 | 10.9 | Hazen collection |
| La Silla Fm, Argentina | AF-23 | 464 | 22.9 | Thompson and Kah 2012 |
| La Silla Fm, Argentina | AF-30 | 464 | 12.4 | Thompson and Kah 2012 |
| La Silla Fm, Argentina | SJF08-14 | 464 | 16.1 | Thompson and Kah 2012 |
| La Silla Fm, Argentina | LFG-27 | 464 | 40.5 | Thompson and Kah 2012 |
| La Silla Fm, Argentina | LFG-55 | 464 | 17.6 | Thompson and Kah 2012 |
| La Silla Fm, Argentina | LS-01 | 464 | 29.7 | Thompson and Kah 2012 |
| La Silla Fm, Argentina | SJC-116 | 464 | 42.1 | Thompson and Kah 2012 |
| West Newfoundland | TH-1 | 464 | 15.3 | Thompson and Kah 2012 |
| West Newfoundland | TH-18 | 464 | 41.7 | Thompson and Kah 2012 |
| Ludlow Fm, Silurian | BH28 | 432 | 30.3 | Hazen collection |
| Clay's Ferry Fm, Kentucky | BH49 | 457 | 7.1 | Hazen collection |
| Limestone Quarry, Dickensonville, Virginia | BH29 | 406 | 7.7 | Hazen collection |
| John Boyd Thatchen State Park, New York | BH30 | 406 | 12.8 | Hazen collection |
| Cincinnati, Ohio | BH32 | 451 | 6.5 | Hazen collection |
| Richmond, Indiana | BH27 | 451 | 7.3 | Hazen collection |
| Blue Stone limestone Quarry, New York | BH34 | 406 | 19.0 | Hazen collection |
| Isle La Motte, Vermont | BH38 | 406 | 21.6 | Hazen collection |
| Isle La Motte, Vermont | BH39 | 406 | 12.2 | Hazen collection |
| Isle La Motte, Vermont | BH40 | 406 | 22.9 | Hazen collection |
| Tenby, Wales | BH43 | 329 | 69.0 | Hazen collection |
| Plainville Quarry, Ohio | BH44 | 388 | 17.4 | Hazen collection |

| | | | | |
|---|---|---|---|---|
| Everett Quarry, Missouri | BH45 | 311 | 15.4 | Hazen collection |
| Cheddar Gorge, England | BH46 | 329 | 65.5 | Hazen collection |
| Mammoth Cave National Park, Kentucky | BH47 | 341 | 190.6 | Hazen collection |
| Sheep Mountain | BH51 | 341 | 53.6 | Hazen collection |
| Limestone Quarry, Ohio | BH52 | 388 | 4.2 | Hazen collection |
| Hamilton Group, New York | BH22 | 388 | 3.6 | Hazen collection |
| Madision limestone, Garrett Co., Maryland | BH23 | 341 | 31.7 | Hazen collection |
| Coral limestone, Michigan | BH53 | 389 | 21.0 | Hazen collection |
| Lydstep Haven coral, Wales | BH35 | 329 | 70.4 | Hazen collection |
| Shark Bay, Australia | BH20 | 0 | 28.4 | Hazen collection |

***SI 2. Data filtering***

Diagenetic alteration can be problematic when interpreting the chemical composition carbonate rocks; therefore, we carefully screened carbonate specimens for a range of diagenetic effects and hydrothermal alteration by combining geologic, petrographic, and element and isotope geochemical analyses. For the published literature, we compiled data only for samples that are considered to reflect primary depositional environments. For our own analyses, we selected samples from within known sedimentological and stratigraphic context, most of which are from previously investigated rock units. Petrographic analysis was used to selected sample areas preserving original sedimentary fabrics, which suggest the least interaction with diagenetic fluids, and samples were microdrilled from these localities. To identify possible affects of diagenesis, we screened the samples based on the classic geochemical tracers of late diagenesis, including major and minor elements (e.g., Fe, Mn, Sr) as well as C and O isotopic signatures. We did not fix the selection criteria; rather, we adopted the selection criteria used by individual researchers for the different localities and published in their original descriptions. Readers can refer to the original papers that describe the samples in the reference lists below (*SI 6. References*). In addition, we studied REE patterns and Eu anomalies to avoid samples with significant hydrothermal alternation (e.g., Frimmel, 2009). Both Zn and Fe partition coefficient ($K_d$) from fluid to carbonates increase with increasing diagenesis as shown by earlier work of Brand and Veizer (1980). Also, $K_d$ (Fe) increases faster compared to $K_d$ (Zn), from 1 to 20 and from 5.2 to 5.5 for Fe and Zn, respectively. So, diagenesis will cause decrease in Zn/Fe ratios by incorporating more Fe than Zn in carbonates. Even though, every carbonates we studied today have been through diagenesis. That is why we are adopting a statistic treatment of our global data.

***SI 3. Statistical analysis of data***

Temporal data sets are subject to biases associated with sampling: recent geological eras are commonly represented by more samples, and some formations are represented by multiple analyses. Since we do not know exactly how the effect of diagenesis, local primary production, mineralogy and kinetic effect influence on the Zn/Fe values, we therefore adopted three discrete approaches to statistically evaluate Zn/Fe data through time aiming to investigate the population behavior. First, we divided the entire sample population into eight bins of different duration to make sure each bin has statistically meaningful sample numbers (where $n > 50$, expect for one, bin with $n = 38$). The bins were chosen to reflect current hypotheses for $pO_2$ evolution through time; specifically, we chose a bin boundary at 800 Ma to reflect the recent hypothesis of Planavsky et al. (2014) concerning mid-Neoproterozoic oxygenation, and we broke out Cryogenian, Ediacaran and Lower Paleozoic bins in an attempt to illuminate existing hypothesis concerning Ediacaran-Cambrian oxygen increase. Each bin contains samples from at least two different geological formations. The choice of the bin breaking points is based on convenience and what is already know about $pO_2$ evolution through Earth history. For example, the first bin is from 3.5 – 2.5 Ga, which is the Pre-GOE time, where we expect low $pO_2$ and we observe low Zn/Fe and little variation of Zn/Fe. We divide the following bin into 2.5-2.0 Ga and 2.0-1.5 Ga, to have statistical meaning number of samples in each bin. Then we have three different formation from ~800 Ma with high Zn/Fe compared to Pre-1.0Ga samples and therefore we make a bin from 1.5-0.8 Ga. For the following time periods, we divide bins into several geological meaningful groups, as 800-635 Ma (Cryogenian), 635-541 Ma (Ediacaran), 541-300 Ma （earlier

Paleozoic), and 300-0 Ma (later Paleozoic, Mesozoic and Cenozoic) to make self-consistent and statistically meaningful sample subsets.

We then performed a box-whisker plot for all data (Fig. S3), where median, 50%, and outliers (outside of 3 sigma of the population) of Zn/Fe values were calculated for each bin, which are shown with red lines (orange lines in Fig. 2), blue boxes, and red crosses, respectively in Fig. S3. In a second approach, we divided data into the same ten bins as in the previous approach, but we plotted histograms for each bin (Fig. S4). Data in nearly all of the bins follows a lognormal distribution, which permits calculation of means and standard deviations for each of the 10 bins (shown with blue lines in Fig. 2). In a third approach, we calculated average composition for each geological formation, which reduces the influence from sampling bias. For example, some localities/formations are represented by 20 samples, whereas others incorporate 10 or fewer. The formation averages are shown in Fig. 2 and a polynomial fit is calculated and displayed in Fig. S5.

***SI 4. Assumptions, deviation of equations and sensitivity tests***

Fe oxidization chemical reaction can be written as:

$4Fe^{2+}$ (aq) + $O_2$ (aq) + $10H_2O$ (aq) = $4Fe(OH)_3$ (s) + $8H^+$ (aq)

$$K = \frac{a^8_{(H^+)}}{a^{10}_{(H_2O)} \times a^4_{(Fe^{2+})} \times a_{(O_2)}} \quad [1],$$

where $K$ is equilibrium constant and $\alpha$ is activity. In this equation, we assume that when $Fe^{2+}$ oxidizes to $Fe^{3+}$ and is precipitated from the aqueous system as iron hydroxide [$Fe(OH)_3$], thus only $Fe^{2+}$ is incorporated into carbonates. Assuming equilibrium between atmosphere and surface ocean on hundredmillion year time scales (the smallest bin size is around 100 million years, Bin6: 635-541 Ma), we replace $\alpha(O_2)$ in equation [1] with oxygen fugacity in the atmosphere, $f_{(O_2)}$, as

$$K = \frac{a^8_{(H^+)}}{a^{10}_{(H_2O)} \times a^4_{(Fe^{2+})} \times f_{(O_2)}} \quad [2].$$

Then we can reorganize equation [2] to

$$logK = 4log\frac{1}{a_{(Fe^{2+})}} - log\, f_{(O_2)} + log\frac{a^8_{(H^+)}}{a^{10}_{(H_2O)}} \quad [3],$$

if we assume the Zn concentrations in seawater and partitioning of Zn/Fe from seawater to carbonate minerals are constant over Earth's history. Therefore, we can write the equation normalized to $Zn^{2+}$ as

$$logK = 4loga^P_{(Zn^{2+}/Fe^{2+})} - log\, f^P_{(O_2)} + log\frac{a^8_{(H^+)}}{a^{10}_{(H_2O)}}$$

$$logK = 4loga^{M}_{(Zn^{2+}/Fe^{2+})} - log\, f^{M}_{(O_2)} + log\frac{a^{8}_{(H^{+})}}{a^{10}_{(H_2O)}} \quad [4],$$

in which superscripts P and M indicate the past and modern parameters. Assuming pH and K are constant, we can simplify the relationship between Fe/Zn ratios and $f_{(O_2)}$, as $f^{P}_{(O_2)} = r^4 \cdot f^{M}_{(O_2)}$ [6], where $f^{P}_{(O_2)}$ is the oxygen fugacity in the past (any time in Earth's history), $f^{M}_{(O_2)}$ is the oxygen fugacity in modern time, and

$$r = \frac{(Fe^{2+}/Zn^{2+})^{M}}{(Fe^{2+}/Zn^{2+})^{P}} = \frac{(Zn^{2+}/Fe^{2+})^{P}}{(Zn^{2+}/Fe^{2+})^{M}} \quad [6],$$

provides Zn/Fe ratios in past carbonate normalized to the modern values. If we assume that atmospheric $O_2$ is in equilibrium with the shallow marine environment, and that we know the current atmospheric $P_{(O_2)}$ (0.21) and the modern seawater Zn/Fe ratios as reflected in Zn/Fe ratios of marine carbonates, we can therefore calculate $f_{(O_2)}$ at any given time of Earth's history if we know the Zn/Fe ratio.

***Discussion of assumptions***

This approach requires several critical assumptions, one of which is that we assume the pH of the ocean has not changed significantly through Earth's history—an assumption supported by some studies (Grotzinger and Kasting, 1993; Sumner and Grotzinger, 2004). However, we do recognize the possible great influence of pH change on quantitative constraint of atmospheric $O_2$. We also assume a constant Zn concentration in seawater through time. Although Zn concentrations, theoretically may have responded to changes in enzymatic use during biosphere evolution, there is no evidence for change in Zn bioavailability change through time (Robbins et al., 2013; Scott et al., 2013). However, Zn

concentrations in seawater may drop during the Mid-Proterozoic due to some extent of euxinia (~1~10 % of modern seafloor area) (Reinhard et al., 2013). These two important factors (pH and Zn content) may contribute on various degrees to the accuracy of atmospheric $O_2$ estimation in our model. However, we do not have a quantitative understanding of either at present. Therefore, we develop a first order quantification of secular evolution of atmospheric $O_2$ with the assumptions that neither pH nor Zn content in seawater change significantly during the time intervals we investigated.

***Sensitivity tests of the modeling***

Here, we evaluate how temperature and pH changes influence the modeling results in seawater through Earth's history.

First, we perform a sensitivity test that assuming three different ***temperatures***:

$Fe^{2+} + CaCO_3 \text{ --> } Ca^{2+} + FeCO_3$ [1]

$Zn^{2+} + CaCO_3 \text{ --> } Ca^{2+} + ZnCO_3$ [2]

By combining eqn (1) and (2), we have $FeCO_3 + Zn^{2+} \text{ --> } ZnCO_3 + Fe^{2+,}$ where equilibrium constant K can be written as $\log K = \log (a(ZnCO_3)/a(FeCO_3)) - \log (a(Zn^{2+})/a(Fe^{2+}))$, where a are activities for different components. We then calculate K values at different temperatures using SUPCRT92 (Johnson et al., 1992) and the results are shown in the following figure.

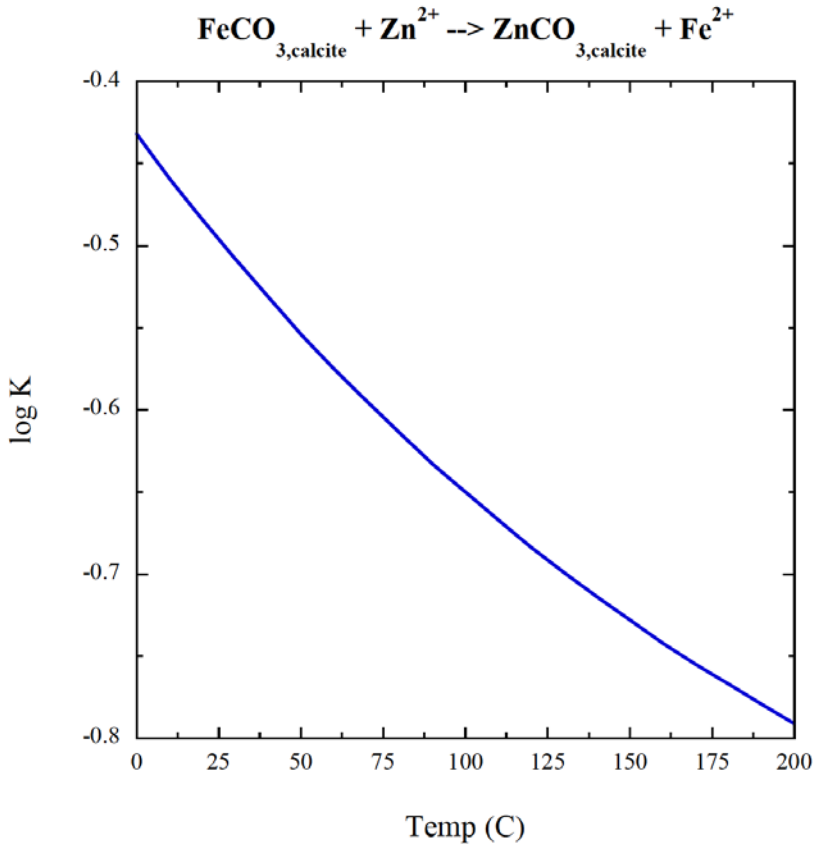


Generally, when T increases, log K (also K) decreases, but still not so much.

For example,

When T = 25 $^{o}$C, log K = -0.496, K = 0.32;

When T = 60 $^{o}$C, log K = -0.575, K = 0.27;

When T = 100 $^{o}$C, log K = -0.65, K = 0.22.

If we take the most extreme example: Assuming modern T is 25$^{o}$c and Archean T is 100$^{o}$C. The $fO_2$ estimate in the Archean will increase by approximately 40%. Therefore, even if we assume the most extreme ocean temperature (100$^{o}$C), the uncertainty caused by temperature

change on $fO_2$ estimate is much smaller compared to uncertainties generated by Zn/Fe variations in carbonates (Figure 3), which is at least one order of magnitude.

Second, we carry out a sensitivity test on ***pH*** change:

$$logK = 4loga^{P}_{\left(\frac{Zn^{2+2+}}{Fe}\right)} - log\, f^{P}_{(O_2)} + log\, \frac{a^{8}_{(H^+)}}{a^{10}_{(H_2O)}}^{P}$$

$$logK = 4loga^{M}_{(Zn^{2+}/Fe^{2+})} - log\, f^{M}_{(O_2)} + log\, \frac{a^{8}_{(H^+)}}{a^{10}_{(H_2O)}}^{M}$$

The modern day seawater has a pH of ~8 (M in the equation). If we assume a lower pH in the past (P in the equation), we can rearrange the equations as

$$4loga^{P}_{(Zn^{2+}/Fe^{2+})} - log\, f^{P}_{(O_2)} + log\, \frac{a^{8}_{(H^+)}}{a^{10}_{(H_2O)}}^{P} = 4loga^{M}_{(Zn^{2+}/Fe^{2+})} - log\, f^{M}_{(O_2)} + log\, \frac{a^{8}_{(H^+)}}{a^{10}_{(H_2O)}}^{M}$$

$$\frac{a^{P}_{(Zn^{2+}/Fe^{2+})}{}^{4}\, a^{P}_{(H^+)}{}^{10}}{a^{P}_{(H_2O)}{}^{10}\, f^{P}_{(O_2)}} = \frac{a^{M}_{(Zn^{2+}/Fe^{2+})}{}^{4}\, a^{M}_{(H^+)}{}^{10}}{a^{M}_{(H_2O)}{}^{10}\, f^{M}_{(O_2)}}$$

Final, we get the new pH dependent relationship as

$$f^{P}_{(O_2)} = \frac{a^{P}_{(Zn^{2+}/Fe^{2+})}{}^{4}}{a^{M}_{(Zn^{2+}/Fe^{2+})}{}^{4}} \left(\frac{a^{P}_{(H^+)}}{a^{M}_{(H^+)}}\right)^{8} f^{M}_{(O_2)}$$

Therefore, if the pH is lower in the past, this will cause the $O_2$ estimate to be lower. This also means that the $O_2$ level we estimate is the maximum values assuming the pH was lower in the past. Also, if we change the pH from 8.1 to 7.6, estimated $O_2$ is four orders of magnitude lower because the $O_2$ estimate is sensitive pH change. Since we do not know how seawater

pH change through time, and there is no evidence that it changes dramatically on the order of hundreds of million years, we keep the pH constant in our model. However, if we understand better how pH change through time, we can plug in pH in above equations and get a more accurate estimate of $O_2$ evolution through time.

*SI 5. Figures*

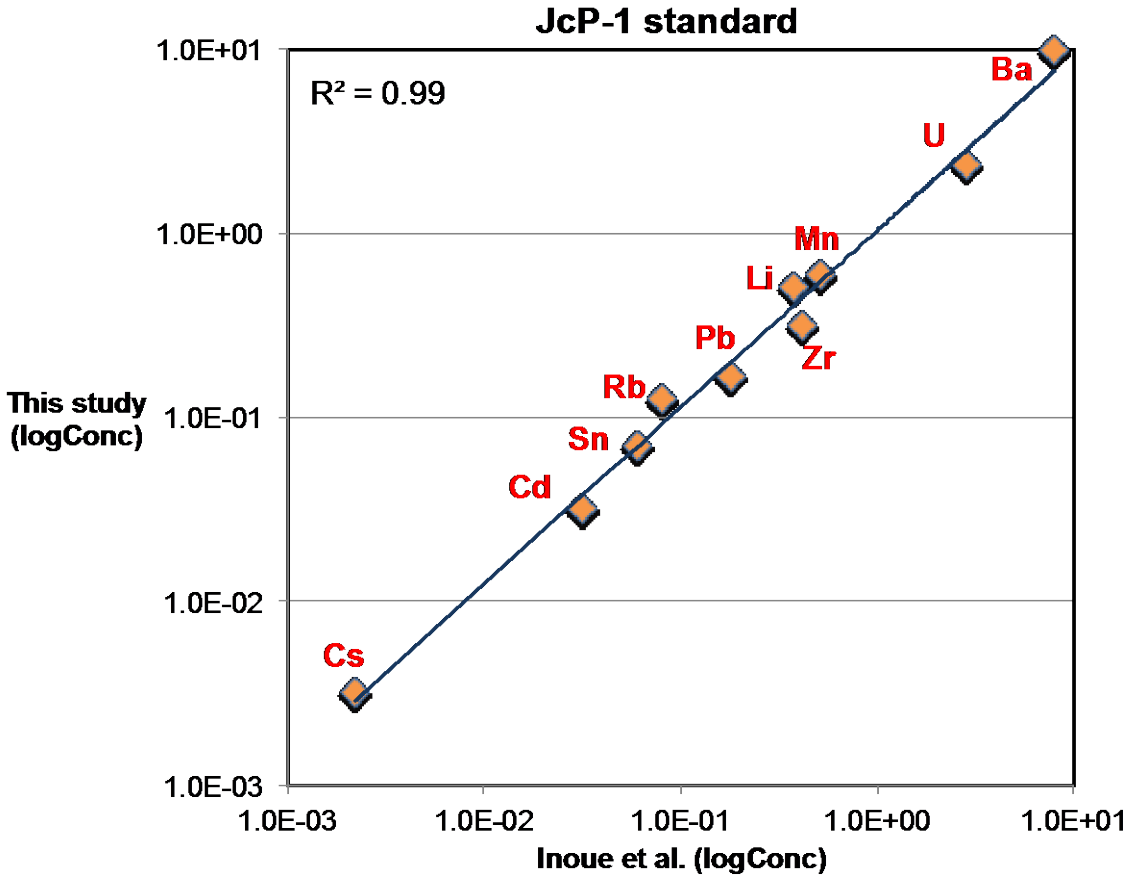


Figure S1. Comparison of measured trace elements with those reported for Inoue et al. (2004) for the JcP-1 standard. The full analytical method is discussed in the method section fallowing the main text.

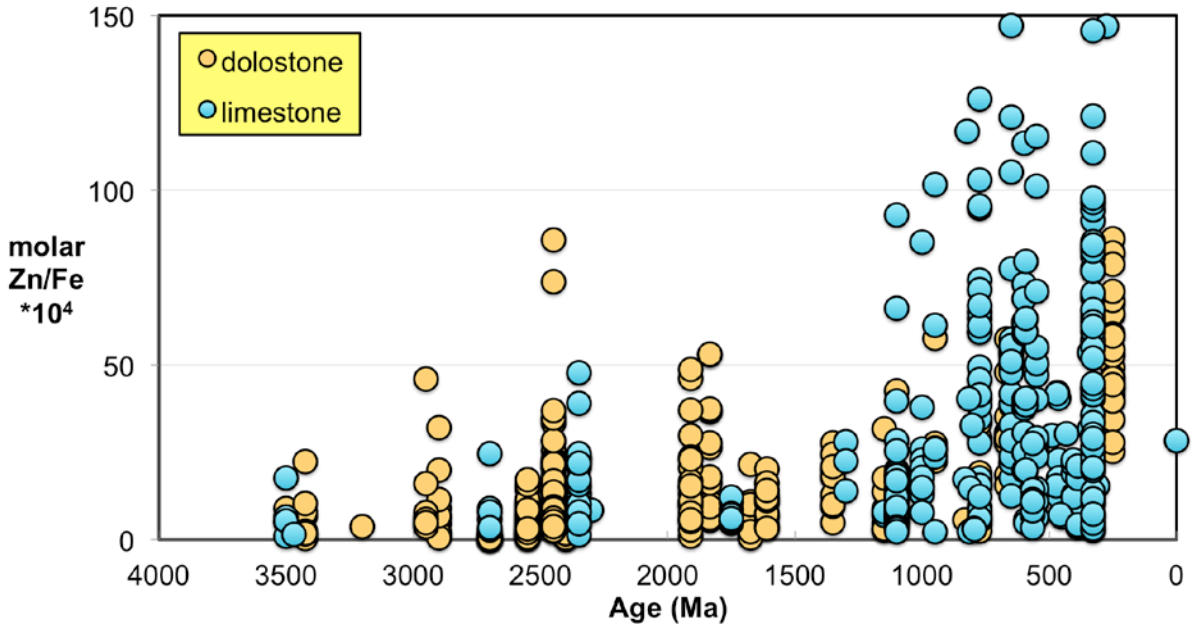


Figure S2. Zn/Fe ratios in marine carbonate, plotted with information on sample lithology.

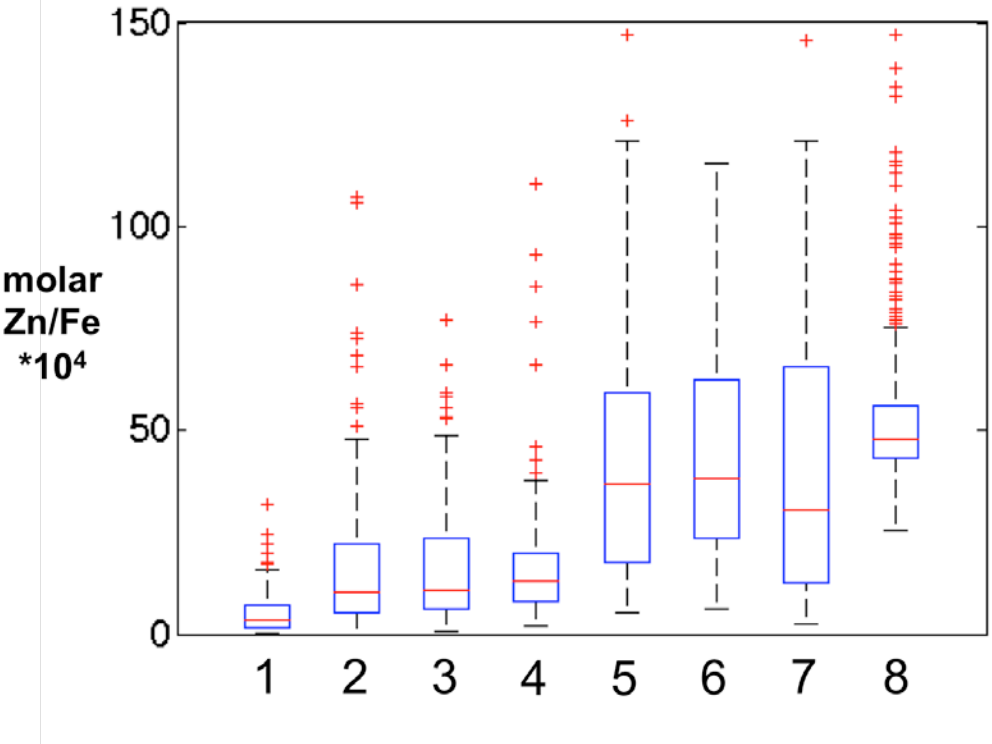


Figure S3. Box-whisker distribution of all samples. The sample population is divided into eight bins (Bin1: 3.5 -2.5 Ga, Bin2: 2.5-2.0 Ga, Bin3: 2.0-1.5 Ga, Bin4: 1.5-0.8Ga, Bin5: 800-635 Ma, Bin6: 635-541Ma, Bin7: 541-300Ma, Bin8: 300-0 Ma) of different duration to make sure each bin has statistically meaningful sample numbers (where n > 50, expect for one, bin with n = 38). Each bin contains samples from at least two different geological formations. We show a Box-whisker plot for each group. Median values are indicated by the red lines and each individual boxes include 50% samples and whiskers mark the 3 sigma boundaries of the group population. Red crosses fall out of whiskers and are considered outliers.

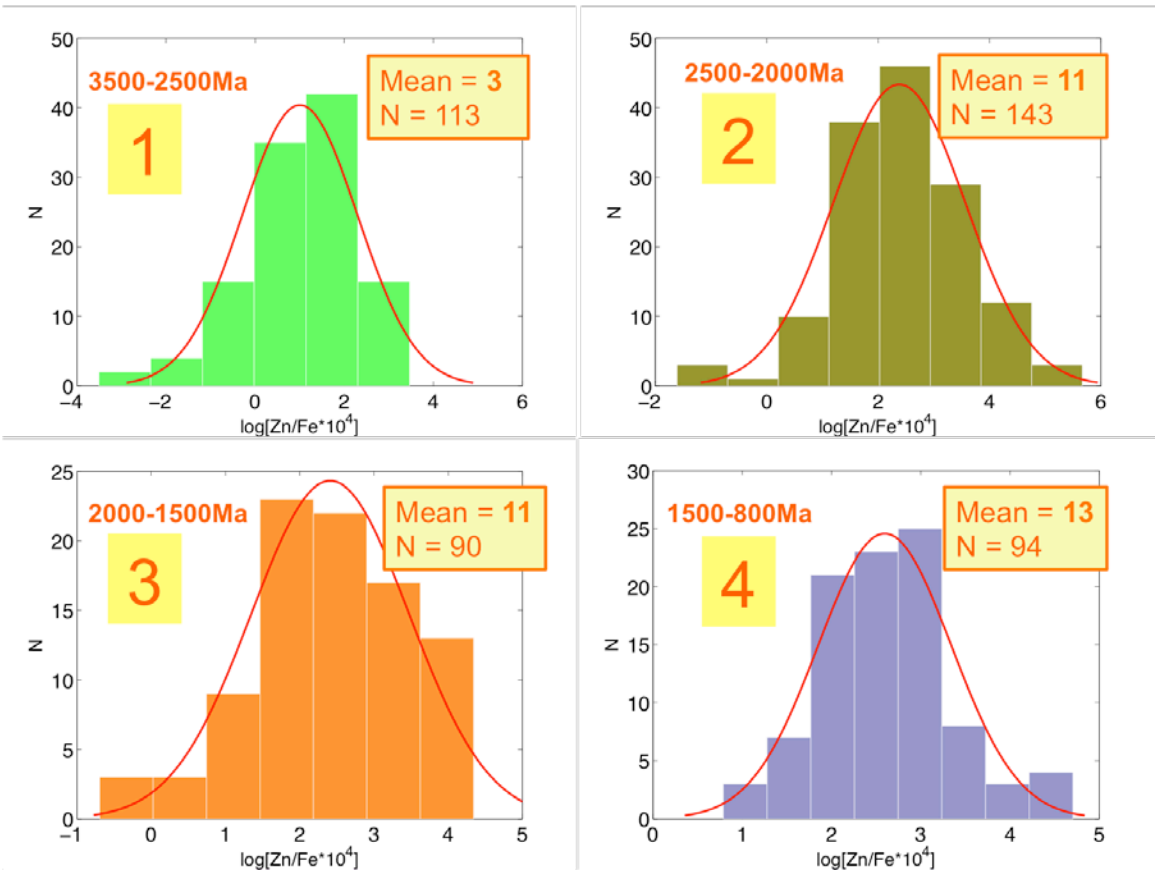
3500-2500Ma
1
Mean = 3
N = 113
2500-2000Ma
2
Mean = 11
N = 143
2000-1500Ma
3
Mean = 11
N = 90
1500-800Ma
4
Mean = 13
N = 94
N
log[Zn/Fe*10^4]

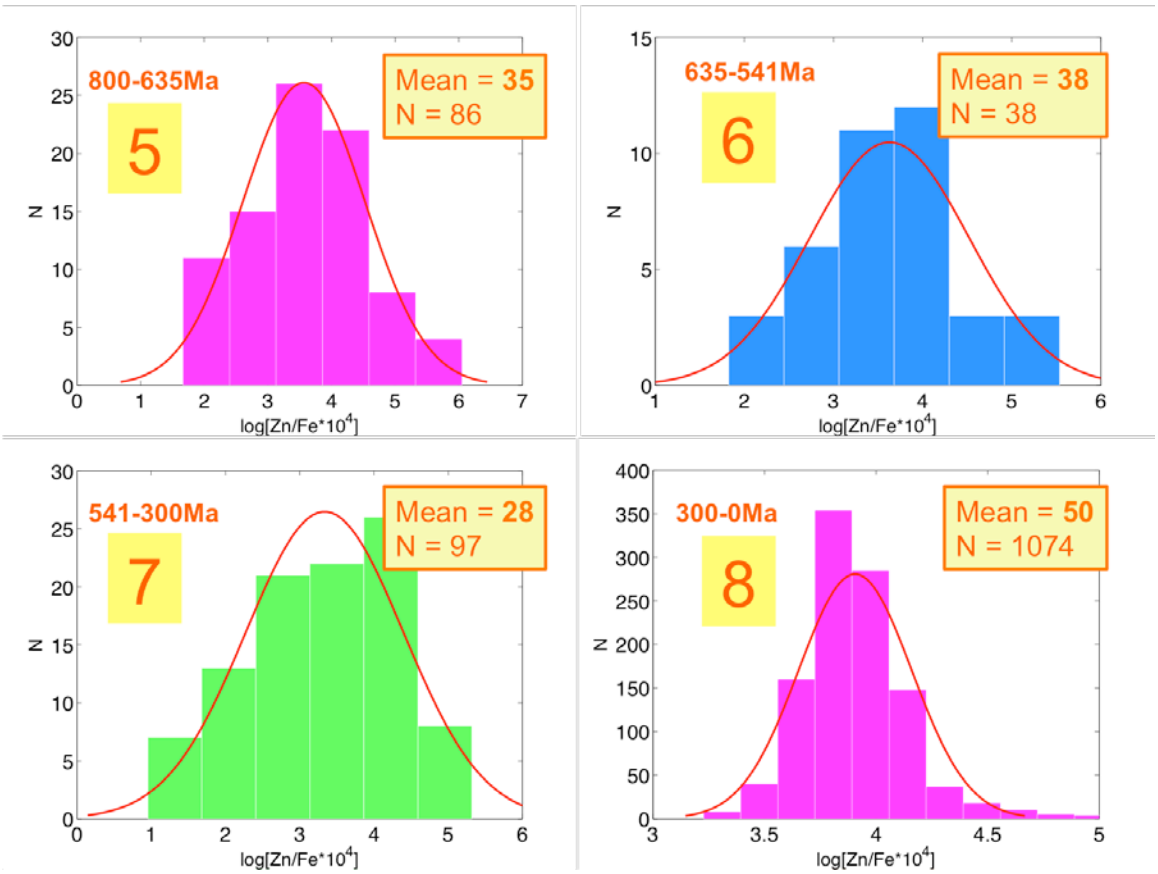


Figure S4. Histograms of Zn/Fe ratios with lognormal fitting in red. We group all data into eight different bins (age distribution of the bins is provided in Fig. S2) and plot the lognormal distribution for each group.

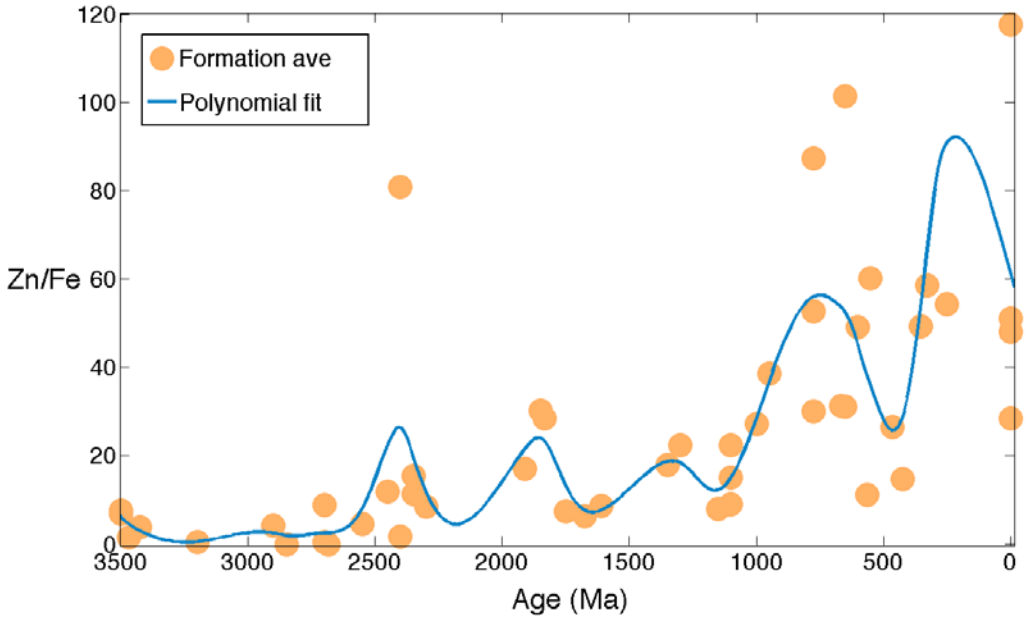


Figure S5. Zn/Fe molar ratio versus time for carbonates averaged by formation. A polynomial fit through the formation average data.

## *SI 6. References*


Bartley, J.K., Kah, L.C., McWilliams, J.L., Stagner, A.F., 2007. Carbon isotope chemostratigraphy of the Middle Riphean type section (Avzyan Formation, Southern Urals, Russia): Signal recovery in a fold-and-thrust belt. Chemical Geology 237, 211-232.

Beukes, N.J., Lowe, D.R., 1989. Environmental control on diverse stromatolite morphologies in the 3000 Myr Pongola Supergroup, South Africa. Sedimentology 36, 383-397.

Bickford, M.E., Basu, A., Patranabis-Deb, S., Dhang, P.C., Schieber, J., 2011. Depositional History of the Chhattisgarh Basin, Central India: Constraints from New SHRIMP Zircon Ages. Journal of Geology 119, 33-50.

Chakrabarti, G., Shome, D., Kumar, S., Stephens, G.M., III, Kah, L.C., 2014. Carbonate platform development in a Paleoproterozoic extensional basin, Vempalle Formation, Cuddapah Basin, India. Journal of Asian Earth Sciences 91, 263-279.

Cui, H., Kaufman, A.J., Xiao, S., Zhu, M., Zhou, C., Liu, X.-M., 2014. Redox architecture of an Ediacaran ocean margin: Integrated chemo-stratigraphic ($\delta^{13}C$–$\delta^{34}S$–$^{87}Sr/^{86}Sr$–Ce/Ce*) correlation of the Doushantuo Formation. Chemical Geology in revision.

Fio, K., Spangenberg, J.E., Vlahovic, I., Sremac, J., Velic, I., Mrinjek, E., 2010. Stable isotope and trace element stratigraphy across the Permian-Triassic transition: A redefinition of the boundary in the Velebit Mountain, Croatia. Chemical Geology 278, 38-57.

Gilleaudeau, G.J., Kah, L.C., 2013. Carbon isotope records in a Mesoproterozoic epicratonic sea: Carbon cycling in a low-oxygen world. Precambrian Research 228, 85-101.

Grotzinger, J.P., Kasting, J.F., 1993. New constraints on precambrian ocean composition. Journal of Geology 101, 235-243.

Inoue, M., Nohara, M., Okai, T., Suzuki, A., Kawahata, H., 2004. Concentrations of trace elements in carbonate reference materials coral JCp-1 and giant clam JCt-1 by Inductively Coupled Plasma-Mass Spectrometry. Geostandards and Geoanalytical Research 28, 411-416.

Jones, D.S., Maloof, A.C., Hurtgen, M.T., Rainbird, R.H., Schrag, D.P., 2010. Regional and global chemostratigraphic correlation of the early Neoproterozoic Shaler Supergroup, Victoria Island, Northwestern Canada. Precambrian Research 181, 43-63.

Kah, L.C., Bartley, J.K., Frank, T.D., Lyons, T.W., 2006. Reconstructing sea-level change from the internal architecture of stromatolite reefs: an example from the Mesoproterozoic Sulky Formation, Dismal Lakes Group, arctic Canada. Canadian Journal of Earth Sciences 43, 653-669.

Kah, L.C., Bartley, J.K., Teal, D.A., 2012. Chemostratigraphy of the Late Mesoproterozoic Atar Group, Taoudeni Basin, Mauritania: Muted isotopic variability, facies correlation, and global isotopic trends. Precambrian Research 200, 82-103.

Kah, L.C., Crawford, D.C., Bartley, J.K., Kozlov, V.I., Sergeeva, N.D., Puchkov, V.N., 2007. C- and Sr-isotope chemostratigraphy as a tool for verifying age of Riphean deposits in the Kama-Belaya aulacogen, the east European platform. Stratigraphy and Geological Correlation 15, 12-29.

Kaufman, A.J., Sial, A.N., Frimmel, H.E., Misi, A., 2009. Neoproterozoic to Cambrian Palaeoclimatic Events in Southwestern Gondwana, in: Gaucher, C., Sial, A.N., Frimmel, H.E., Halverson, G., P. (Eds.), Developments in Precambrian Geology. Elsevier, pp. 369-388.

Knoll, A.H., Hayes, J.M., Kaufman, A.J., Swett, K., Lambert, I.B., 1986. Secular variation in carbon isotope ratios from upper proterozoic successions of svalbard and east greenland. Nature 321, 832-838.

Knoll, A.H., Swett, K., 1990. Carbonate deposition during the late proterozoic era - an example from Spitsbergen. American Journal of Science 290A, 104-132.

Meyer, E.E., Quicksall, A.N., Landis, J.D., Link, P.K., Bostick, B.C., 2012. Trace and rare earth elemental investigation of a Sturtian cap carbonate, Pocatello, Idaho: Evidence for ocean redox conditions before and during carbonate deposition. Precambrian Research 192-95, 89-106.

Miller, N., Johnson, P.R., Stern, R.J., 2008. Marine versus non-marine environments for the Jibalah Group, NW Arabian shield: A sedimentologic and geochemical survey and report of possible metazoa in the Dhaiqa formation. Arabian Journal for Science and Engineering 33, 55-77.

Mirota, M.D., Veizer, J., 1994. Geochemistry of Precambrian carbonates. 6. Aphebian Albanel Formations, Quebec, Canada. Geochimica et Cosmochimica Acta 58, 1735-1745.

Misi, A., Kaufman, A.J., Veizer, J., Powis, K., Azmy, K., Boggiani, P.C., Gaucher, C., Teixeira, J.B.G., Sanches, A.L., Iyer, S.S.S., 2007. Chemostratigraphic correlation of neoproterozoic successions in South America. Chemical Geology 237, 143-167.

Morgan, R., Orberger, B., Rosiere, C.A., Wirth, R., Carvalho, C.d.M., Bellver-Baca, M.T., 2013. The origin of coexisting carbonates in banded iron formations: A micro-mineralogical study of the 2.4 Ga Itabira Group, Brazil. Precambrian Research 224, 491-511.

Planavsky, N.J., Reinhard, C.T., Wang, X., Thomson, D., McGoldrick, P., Rainbird, R.H., Johnson, T., Fischer, W.W., Lyons, T.W., 2014. Low Mid-Proterozoic atmospheric oxygen levels and the delayed rise of animals. Science 346, 635-638.

Reinhard, C.T., Planavsky, N.J., Robbins, L.J., Partin, C.A., Gill, B.C., Lalonde, S.V., Bekker, A., Konhauser, K.O., Lyons, T.W., 2013. Proterozoic ocean redox and biogeochemical stasis. Proc. Natl. Acad. Sci. U. S. A. 110, 5357-5362.

Robbins, L.J., Lalonde, S.V., Saito, M.A., Planavsky, N.J., Mloszewska, A.M., Pecoits, E., Scott, C., Dupont, C.L., Kappler, A., Konhauser, K.O., 2013. Authigenic iron oxide proxies for marine zinc over geological time and implications for eukaryotic metallome evolution. Geobiology 11, 295-306.

Scott, C., Planavsky, N.J., Dupont, C.L., Kendall, B., Gill, B.C., Robbins, L.J., Husband, K.F., Arnold, G.L., Wing, B.A., Poulton, S.W., Bekker, A., Anbar, A.D., Konhauser, K.O., Lyons, T.W., 2013. Bioavailability of zinc in marine systems through time. Nature Geoscience 6, 125-128.

Sergeev, V.N., Knoll, A.H., Petrov, P.Y., 1997. Paleobiology of the Mesoproterozoic-Neoproterozoic transition: The Sukhaya Tunguska Formation, Turukhansk Uplift, Siberia. Precambrian Research 85, 201-239.

Sumner, D.Y., Grotzinger, J.P., 2004. Implications for Neoarchaean ocean chemistry from primary carbonate mineralogy of the Campbellrand-Malmani Platform, South Africa. Sedimentology 51, 1273-1299.

Thompson, C.K., Kah, L.C., 2012. Sulfur isotope evidence for widespread euxinia and a fluctuating oxycline in Early to Middle Ordovician greenhouse oceans. Palaeogeography Palaeoclimatology Palaeoecology 313, 189-214.

Veizer, J., Clayton, R.N., Hinton, R.W., 1992a. Geochemistry of Precambrian carbonates .4. Early Paleoproterozoic (2.25 +/- 0.25 ga) seawater. Geochimica et Cosmochimica Acta 56, 875-885.

Veizer, J., Clayton, R.N., Hinton, R.W., Vonbrunn, V., Mason, T.R., Buck, S.G., Hoefs, J., 1990. Geochemistry of Precambrian carbonates. 3. Shelf seas and nonmarine environments of the Archean. Geochimica et Cosmochimica Acta 54, 2717-2729.

Veizer, J., Hoefs, J., Lowe, D.R., Thurston, P.C., 1989a. Geochemistry of precambrian carbonates. 2. Archean greenstone belts and archean sea-water. Geochimica et Cosmochimica Acta 53, 859-871.

Veizer, J., Hoefs, J., Ridler, R.H., Jensen, L.S., Lowe, D.R., 1989b. Geochemistry of Precambrian carbonates . 1. Archean hydrothermal systems. Geochimica et Cosmochimica Acta 53, 845-857.

Veizer, J., Plumb, K.A., Clayton, R.N., Hinton, R.W., Grotzinger, J.P., 1992b. Geochemistry of Precambrian carbonates. 5. Late Paleoproterozoic seawater. Geochimica et Cosmochimica Acta 56, 2487-2501.

Wilson, J.P., Fischer, W.W., Johnston, D.T., Knoll, A.H., Grotzinger, J.P., Walter, M.R., McNaughton, N.J., Simon, M., Abelson, J., Schrag, D.P., Summons, R., Allwood, A., Andres, M., Gammon, C., Garvin, J., Rashby, S., Schweizer, M., Watters, W.A., 2010. Geobiology of the late Paleoproterozoic Duck Creek Formation, Western Australia. Precambrian Research 179, 135-149.

Zhao, M.-Y., Zheng, Y.-F., 2014. Marine carbonate records of terrigenous input into Paleotethyan seawater: Geochemical constraints from Carboniferous limestones. Geochimica Et Cosmochimica Acta 141, 508-531.

Brand, U., Veizer, J., 1980. Chemical diagenesis of a multicomponent carbonate system; 1, Trace elements. Journal of Sedimentary Research, 50(4): 1219-1236.

Frimmel, H.E., 2009. Trace element distribution in Neoproterozoic carbonates as palaeoenvironmental indicator. Chemical Geology, 258(3-4): 338-353.

Grotzinger, J.P., Kasting, J.F., 1993. New constraints on precambrian ocean composition. Journal of Geology, 101(2): 235-243.

Johnson, J.W., Oelkers, E.H., Helgeson, H.C., 1992. SUPCRT92: A software package for calculating the standard molal thermodynamic properties of minerals, gases, aqueous species, and reactions from 1 to 5000 bar and 0 to 1000°C. Computers & Geosciences, 18(7): 899-947.

Reinhard, C.T. et al., 2013. Proterozoic ocean redox and biogeochemical stasis. Proceedings of the National Academy of Sciences of the United States of America, 110(14): 5357-5362.

Robbins, L.J. et al., 2013. Authigenic iron oxide proxies for marine zinc over geological time and implications for eukaryotic metallome evolution. Geobiology, 11(4): 295-306.

Scott, C. et al., 2013. Bioavailability of zinc in marine systems through time. Nature Geoscience, 6(2): 125-128.

Sumner, D.Y., Grotzinger, J.P., 2004. Implications for Neoarchaean ocean chemistry from primary carbonate mineralogy of the Campbellrand-Malmani Platform, South Africa. Sedimentology, 51(6): 1273-1299.